ACADEMIC PRESS

Available online at www.sciencedirect.com

SCIENCE DIRECT®

Journal of Sound and Vibration 264 (2003) 1005–1043

JOURNAL OF SOUND AND VIBRATION

www.elsevier.com/locate/jsvi

Estimation of the dynamical properties of polyurethane foam through use of Prony series

R. Singh, P. Davies*, A.K. Bajaj

Ray W. Herrick Laboratories, School of Mechanical Engineering, Purdue University, W. Lafayette, IN 47907-1077, USA

Received 31 January 2001; accepted 23 July 2002

Abstract

A system identification procedure is formulated for estimation of parameters associated with a dynamic model of a single-degree-of-freedom foam-mass system. The foam is modelled as a linear viscoelastic material, whose constitutive law is expressed by an exponential hereditary relaxation kernel. The identification procedure is based on modelling the free response of the system as a Prony series (sum of exponentials terms) and fitting this Prony series to the data. This estimated response model is then utilized to estimate the parameters in the system model based on an explicit solution of the model. The procedure is analyzed for its reliability under different sources of error and uncertainties, such as the presence of weak components and experimental noise, and some modifications are evaluated to improve the robustness of the procedure. Finally, the procedure is applied to experimental data to obtain relevant stiffness, viscous and viscoelastic parameters associated with the system. Variations in values of these parameters as a function of static compression are also investigated.

1. Introduction

Foam is an important engineering material, offering unique advantages in terms of low cost and weight, ease of manufacture and energy absorption properties. It has thus found use in many applications: acoustic absorption, impact retardation, and mechanical damping to name a few. In most modern automobile seats, static comfort and vibration isolation are now achieved through the use of foam alone. The realization of the potential of foam as an important engineering material has inspired a close scrutiny of its structure and properties [1–3].

*Corresponding author. Tel.: +1-765-494-9274; fax: +1-765-494-0787.
E-mail address: daviesp@ecn.purdue.edu (P. Davies).

0022-460X/03/$ - see front matter
doi:10.1016/S0022-460X(02)01186-0

1.1. Mechanical properties of foam

As an engineering material, foam has been found to be a non-linear, viscoelastic material whose static and dynamic behavior are sensitive to many variables, such as level of compression and amplitude and frequency of excitation. The non-linear behavior of foam under compression manifests itself in large variations in its local stiffness or elastic modulus as a function of the compressive strain. Such a change can be attributed to the structural and chemical changes that occur as the foam is compressed and exercised [2,4,5]. Exercising the foam results in heat generation, and temperature changes affect the chemical properties of the polymer bonds [4]. Furthermore, for a given compression level, the large amplitude dynamics differ from those under small amplitudes of excitation.

Viscoelasticity of the foam manifests itself in different ways, such as gradual deformation of a block of foam under constant stress (creep behavior), and stress relaxation in the block when it is subjected to a constant strain. In general, viscoelasticity is a phenomenon associated with time variations in a material's response [6]. Thus, the instantaneous stress in the material depends upon both the instantaneous strain and the rate of the strain, as well as higher time derivatives of the strain. As a consequence of such stress–strain relations, foam typically possesses several time constants, some of them quite long, which result in the material taking a long time to achieve its steady state. In the case of dynamic loading, the strain rate, the excitation frequency, the duration of excitation, and the recovery time all affect how the foam responds to a mechanical input. Furthermore, the dynamic stiffness of the foam differs from the static one and shows dependence on the mean level of compression. The viscoelastic properties of foam are also known to be sensitive to humidity and temperature [4,5].

1.2. Mathematical models for foam behavior

In an attempt to describe some of the above effects mathematically, numerous analytical models have been proposed. The modelling efforts vary from simple data-fitting to developing micro-level constitutive relations. Several constitutive laws have been proposed which describe the stress–strain relations in terms of quantities like creep compliance, relaxation modulus, the storage and loss moduli and dynamic viscosity. Some of these constitutive laws have been developed with the aid of mechanical models consisting of combinations of springs and viscous dashpots. The well-known Voigt, Maxwell [6], Kelvin [7], and Wiechart [8] models are representative examples of such models. Some other laws have been derived directly from considerations of continuum mechanics principles [9,10].

The models of viscoelasticity have traditionally used a hereditary approach where the stress in the material is considered a function of the current state of strain, as well as past history of strain in the material. Convolution integral type models are the most widely used models based on this approach, where the stress is assumed to be given by the convolution of strain-rate history with a weighting function, called *relaxation function* [6]. Although the relaxation function can, in general, be a non-linear function of strain as well as time, for small displacements it can be assumed to be independent of the material strain, yielding a linear model. The linear law governing the stress σ and the strain ε under uniaxial loading of the material

is [11]

$$\sigma(t) = \int_0^t G(t-\tau)\dot{\varepsilon}(\tau)\,\mathrm{d}\tau, \tag{1}$$

where $G(t)$ is the relaxation function. An alternative form of this expression in terms of strain history is

$$\sigma(t) = E\left(\varepsilon(t) - \int_0^t \Gamma(t-\tau)\varepsilon(\tau)\,\mathrm{d}\tau\right), \tag{2}$$

where $\Gamma(t-\tau)$ is a difference type relaxation kernel of the material and E is the instantaneous Young's modulus. The lower limit of the integral is zero under the assumption that the strain is first imposed at time $t = 0$.

It has been shown that, if a rational transfer function between stress and strain is assumed for the linear hereditary material, the relaxation kernel consists of a sum of exponentials [12,13]:

$$\Gamma(t) = \sum_{i=1}^{N} a_i \mathrm{e}^{-\alpha_i t}. \tag{3}$$

This form of kernel has been most popular because of its simplicity, and because it has a clear physical interpretation in terms of the time constants $\tau_i = \alpha_i^{-1}$ associated with the response of the viscoelastic material. The time constants essentially quantify the relaxation or creep behavior of a viscoelastic substance. In models with several Maxwell units in parallel, a time constant τ_i is the time required by ith spring to attain its equilibrium state [6]. A viscoelastic solid such as foam may possess a large number of time constants ranging from very small (order of fractions of a second) to very long (several days).

1.2.1. *Mechanics of a dynamical system with foam as an element*

For a dynamic system that incorporates foam only as a component, it is necessary to identify the contribution of the foam in terms of structural parameters like inertia, damping, and stiffness of the complete system. The choice of the model or the form of the constitutive law for the foam is then guided by the loading conditions, application at hand, and ease of incorporation into a structural equation of motion which may include foam as an element. In a dynamic system with a hereditary viscoelastic model for the foam, the equation of motion takes the form of an integro-differential equation. For a system with an external mass element, such as a heavy rigid block riding on the foam, the inertia of the foam can be neglected. The constitutive law for the foam, given by Eq. (2), however still needs to be modified to incorporate a viscous damping term. Such an (integro-differential) equation of motion for the mass-foam system, which contains inertia, viscous damping, stiffness, and viscoelastic parameters, is studied here [14]. As shown by Muravyov and Hutton [15], and given in Section 2, the initial condition response of this system can be expressed as a sum of $N + 2$ exponentials, where N is the number of exponential terms in the relaxation kernel. The coefficients in this response are an implicit function of the model parameters and can thus form a basis to identify the system parameters.

1.3. System identification technique

The parameters of a dynamical system can be estimated by an identification technique that uses the response of the system to external excitations. The identification procedure is guided, of course, by the choice of the model and availability of suitable measurements of inputs and responses. In the case of linear models, an identification procedure can be easily formulated because of availability of the transform techniques. However, a major concern, even in linear cases, is the robustness of the procedure so that accurate estimates of the desired parameters may be obtained in presence of external disturbances and measurement errors.

The present study concerns development of a robust system-identification technique for estimating the material constants associated with the single-degree-of-freedom model for a foam-mass system proposed by White et al. [14]. The technique utilizes the transient response of the system. A linear model is considered under the assumption that the amplitudes of initial displacement as well as system response are sufficiently small.

1.3.1. Prony's method

The identification technique is based on modelling the free acceleration response of the system about an equilibrium position as a sum of a finite number of exponential terms. Since a Prony series is a sum of exponentials model, the procedure of fitting the model to the data is commonly referred to as Prony's method. Note that this model form is consistent with the form of solution derived for the dynamical system model [15]. If samples of a sequence $\{y_n\}$ are available, a Prony's model predicts y_n with a sum of L complex exponentials [16]:

$$\hat{y}_n = \sum_{k=1}^{L} A_k e^{[(\alpha_k + i2\pi f_k)nT + i\theta_k]}, \tag{4}$$

for $0 \leqslant n \leqslant M-1$, where T is the sampling interval in s, A_k are the amplitudes of the complex exponentials, α_k are the decay factors (s^{-1}), f_k are the damped natural frequencies in Hz, θ_k are the initial phases in rad, and i denotes $\sqrt{-1}$. Here it has been assumed in the formulation that the exponentials occur in complex conjugate pairs because that is typically what was found in models of the experimental data. However, the estimation method, described below, does not restrict the model to only have complex conjugate pairs of exponentials and some of the exponentials in the model could be real.

In order to utilize the results of Prony's method for the current problem, the discrete form of the system's free response is expressed as a sum of exponentials

$$x_n = \sum_{k=1}^{L} C_k e^{(p_k T)n}, \tag{5}$$

where T is the sampling interval. Comparing Eqs. (4) and (5) for coefficients gives

$$C_k = A_k e^{i\theta_k} \quad \text{and} \quad p_k = \alpha_k + i2\pi f_k \tag{6}$$

for $k = 1, 2, \ldots, L$. If $x(nT)$ is the sampled impulse response, $h(nT)$, of the system, then its z-transform, the discrete system's transfer function ($H(z)$), is a ratio of polynomials. Thus, in essence, the response is being modelled as an auto-regressive moving average (ARMA) process. This approach is fundamentally similar to that used by Yu and Haddad [17,18].

The estimation of the parameters of a Prony series model consists of three steps [16]. In the first step, the response at one time is modelled as a weighted sum of the response at previous times. The weights, or linear prediction parameters, are determined through a linear least-squares fit to the data. This is akin to the algorithms used in AR and ARMA model parameter estimation [16]. In the second step, the zeros of a so-called linear prediction polynomial, whose coefficients are the linear prediction parameters of step 1, are determined. These two steps essentially constitute the process of determination of the poles of an auto-regressive (AR) model of the data. The zeros of the prediction polynomial are thus also called the *poles* of the model, as they are in AR estimation. In the third step, a set of linear equations, functions of the poles estimated in step 2 and the response data, is solved in a least-squares sense to determine the amplitudes of the Prony series terms; these are also the residues associated with each of the model poles.

The identification technique thus formulated on the basis of Prony's method, is then analyzed for its reliability with experimental data. Several sources of errors and uncertainties are identified, such as the presence of low-amplitude components and noise, and suitable remedies to overcome the associated problems are evaluated by means of numerical simulations. Higher order models, which increase the model span (LT) and allow for modelling of the noise structure, were found to be useful in improving parameter estimates and identifying low-amplitude components in the model. The resulting identification process is shown to be robust. The identification technique is finally applied to acceleration response data from a free-vibration experiment, and the parameters of the foam model in uniaxial compression are estimated under different system configurations. A static-creep experiment is also performed to estimate the longer time constants associated with the foam block.

2. Formulation of problem and solution procedure

A dynamic viscoelastic foam-mass system constrained to undergo linear unidirectional motion, as shown in Fig. 1, can be modelled as a single-degree-of-freedom system. The equation of motion of this system, as considered by White et al. [14], is

$$m\ddot{x} + c\dot{x} + kx + k_3x^3 + k_5x^5 - k\int_{-\infty}^{t} \Gamma(t-\tau)x(\tau)\,\mathrm{d}\tau = f(t), \tag{7}$$

where $x(t)$ represents the absolute vertical displacement of the top mass from its static equilibrium configuration, c is the viscous damping coefficient, k, k_3 and k_5 are the linear, cubic and fifth order stiffness terms, and $\Gamma(t-\tau)$ is the relaxation kernel for which a sum of exponential model (Eq. (3)) is used. Here, $f(t)$ represents a general forcing term which may include contributions from external excitation and dry friction. For a free vibration experiment with negligible dry friction, $f(t) = 0$. Furthermore, if the amplitude of response is small, the cubic and fifth order terms can be neglected (a technique to identify the full non-linear model is described elsewhere [14]). The equation of motion becomes linear under this small response assumption

$$m\ddot{x} + c\dot{x} + kx - k\int_{0}^{t} \sum_{i=1}^{N} a_i \mathrm{e}^{-\alpha_i(t-\tau)}x(\tau)\,\mathrm{d}\tau = 0, \tag{8}$$

where the lower limit of integration is set to zero under the assumption that the motion starts at $t = 0$. Free responses are generated by means of suitable initial conditions $x(0)$ and $\dot{x}(0)$.

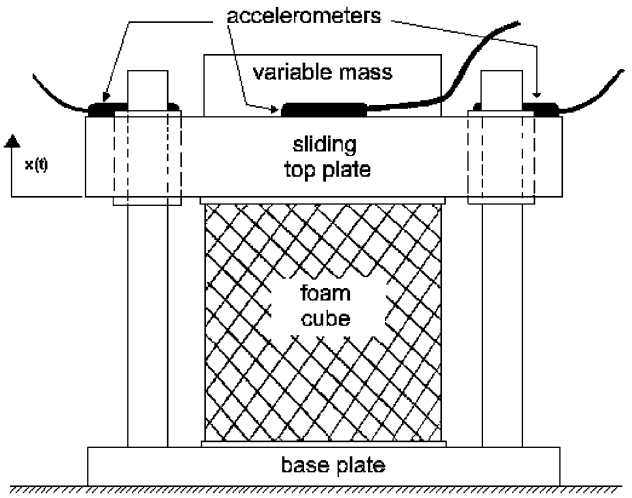

Fig. 1. Schematic diagram of the experimental setup.

Muravyov and Hutton [15] have investigated the analytical solution for the response of this system. The solution process is based on expressing the free response as a sum of $N+2$ complex exponential terms

$$x(t) = \sum_{j=1}^{N+2} C_j e^{p_j t}, \tag{9}$$

where the coefficients C_j are called *residues* in reference to partial fraction expansion of the Laplace transform of the above equation, and p_j are the system eigenvalues. N is the number of terms in the relaxation kernel. By substituting this solution into the equation of motion (Eq. (8)) and setting the sum of the coefficients of each time-dependent exponential term to zero the following equations are obtained:

$$mp_j^2 + cp_j + k\left(1 - \sum_{i=1}^{N} \frac{a_i}{p_j + \alpha_i}\right) = 0, \quad j = 1, 2, \ldots, N+2, \tag{10}$$

$$\sum_{j=1}^{N+2} \left(\frac{a_i}{p_j + \alpha_i}\right) C_j = 0, \quad i = 1, 2, \ldots, N. \tag{11}$$

The relationships for initial conditions are

$$\sum_{j=1}^{N+2} C_j = x_0 \tag{12a}$$

and

$$\sum_{j=1}^{N+2} C_j p_j = \dot{x}_0. \tag{12b}$$

If the initial conditions and system parameters m, c, k, α_i and a_i are already known, Eqs. (10)–(12) can be used to obtain the response parameters C_j and p_j, and thus generate a closed form solution for the response $x(t)$ [15].

For the system identification problem, the task is to use the samples of free vibration response $x(t)$ to calculate the material parameters c, k, α_i and a_i. This is achieved through a three-step process described below:

1. Express the response as a sum of complex exponentials, as given in Eq. (9), and obtain an estimate of the complex coefficients C_j and p_j by using Prony's method.

   Note that in the second stage of the Prony method, the poles are estimates of $e^{p_j T}$, where T is the sampling interval in s. Therefore, it is straightforward to estimate the p_j once estimates of the poles are known. In the last stage of the Prony method the C_j, the coefficients of the Prony series terms, are estimated.
2. Use the estimates of C_j and p_j in Eq. (11) to calculate α_i.

   Eq. (11) can be simplified to

$$\sum_{j=1}^{N+2} \frac{C_j}{p_j + \alpha_i} = 0, \quad i = 1, 2, \ldots, N \tag{13}$$

   and then the $N+2$ partial fractions combined to produce a polynomial in powers of α_i in the numerator. This stage therefore involves generating the numerator polynomial, $P(\alpha_i)$, and finding the roots of $P(\alpha_i) = 0$, i.e.,

$$P(\alpha_i) = \sum_{i=1}^{N+2} C_j \prod_{i=1,\ i \neq j}^{N+2} (p_j + \alpha_i) = 0. \tag{14}$$

   This equation is of order $N+1$ in α_i. Thus there arise $N+1$ roots for N unknowns α_i. This leads to the problem of identifying the N true roots out of a total of $N+1$ roots. The problem is discussed in Section 3.1, where it is shown that the extra root is a function of initial conditions $x(0)$ and $\dot{x}(0)$.
3. If it is assumed that the genuine N roots for α_i are known, the remaining material parameters can be determined by using Eq. (10), which gives rise to a linear set of $N+2$ simultaneous equations in the $N+2$ unknowns c, k and a_i. These equations can be put in a matrix form as

$$\begin{bmatrix} p_1 & 1 & \dfrac{-1}{p_1+\alpha_1} & \cdots & \dfrac{-1}{p_1+\alpha_N} \\ p_2 & 1 & \dfrac{-1}{p_2+\alpha_1} & \cdots & \dfrac{-1}{p_2+\alpha_N} \\ \cdots & \cdots & \cdots & \cdots & \cdots \\ \cdots & \cdots & \cdots & \cdots & \cdots \\ p_{N+2} & 1 & \dfrac{-1}{p_{N+2}+\alpha_1} & \cdots & \dfrac{-1}{p_{N+2}+\alpha_N} \end{bmatrix} \begin{bmatrix} c \\ k \\ \tilde{a}_1 \\ \cdots \\ \tilde{a}_N \end{bmatrix} = -m \begin{bmatrix} p_1^2 \\ p_2^2 \\ \cdots \\ \cdots \\ p_{N+2}^2 \end{bmatrix}, \tag{15}$$

   where $\tilde{a}_i = k a_i$.

Eqs. (13) and (15) constitute the required equations for system identification. The equations for the initial conditions are not explicitly needed, except for identifying the 'spurious' α_i in stage 2.

It is important to note that the samples of displacement response $x(t)$ are not directly available. In actual experiments, the acceleration response $\ddot{x}(t)$ is measured by using accelerometers. Hence, $\ddot{x}(t)$ is first expressed as a sum of complex exponentials

$$\ddot{x}(t) = \sum_{j=1}^{N+2} D_j e^{p_j t}. \tag{16}$$

The displacement response $x(t)$ is calculated from $\ddot{x}(t)$ by integration, assuming stability and that $x(t)$ contains no constant term (that is, a term with $p_j = 0$). Then, the coefficients C_j in Eq. (9) are given by $C_j = D_j/p_j^2$. The coefficients D_j and the frequencies p_j are estimated by using Prony's method on discrete samples of $\ddot{x}(t)$, as discussed in Section 1.3.

3. Theoretical and numerical analysis of identification procedure

In Section 2, a method for identification of system parameters based on Prony's method of modelling the response was developed. In this section, the problems concerning the applicability and reliability of the method, when used to model experimental data, are addressed. The sources of errors and uncertainties are identified and remedies are suggested to make the identification procedure robust in light of these problems. Analysis is carried out for systems with single- ($N = 1$) and two-term ($N = 2$) relaxation kernels. The case of $N = 1$ is chosen for simplicity. For this case, the latter two stages of the system identification procedure can be carried out analytically, since Eq. (14) generates a quadratic equation in α_i. The case $N = 2$ is of special interest since it is generally the order observed in the experimental analysis with the foam-mass system. Numerical simulations were carried out for a system with $N = 2$. The parameter values chosen for simulation were: $m = 1$ kg, $c = 10$ N s/m, $k = 2500$ N/m, $a_{1,2} = -3 \pm 4\text{i}$ s^{-1} and $\alpha_{1,2} = 10 \pm 90\text{i}$ s^{-1}. A sampling frequency of 256 Hz was used for simulations and the simulated time series had, typically, 250–500 samples. These parameters were chosen to generate time histories similar to those observed in the experiments.

3.1. The problem of the spurious α_i

Eq. (14) is a $(N + 1)$th order polynomial in a single variable, and can therefore be written as

$$A_0\beta^{N+1} + A_1\beta^N + A_2\beta^{N-1} + \cdots + A_N\beta + A_{N+1} = 0, \tag{17}$$

where α is the independent variable. An algebraic evaluation was carried out to analyze the specific dependence of α_i on the response coefficients C_j and p_j. The evaluation revealed that, of the $N + 1$ roots of Eq. (17), N are the genuine roots (α_i) and the remaining one is a 'spurious' root, in the sense that its value depends upon the initial conditions $x(0)$ and $\dot{x}(0)$. The expression for this spurious root was found to be

$$\beta = \alpha_{spurious} = \frac{\dot{x}_0}{x_0} + \frac{c}{m} \tag{18}$$

and this result is independent of the number of terms in the relaxation kernel. For the case of $N = 1$, the derivation is presented in Appendix A. In the presence of noise, the expression is more complicated (see Section 3.6). By performing experiments with different initial conditions, it would be possible to recognize and reject the spurious root, since it will be the only root that varies with initial conditions. Furthermore, it may be noted that $A_0 = x(0)\ \forall N$. Thus if the initial displacement $x(0)$ is zero, the spurious root does not arise for any number of terms in the relaxation kernel, since the leading coefficient A_0 in Eq. (17) becomes identically zero. Eq. (13) then yields exactly N roots. This would be the ideal case where the response is initiated by means of an impulse at $t = 0$. However, in real circumstances, as discussed below, it is difficult to realize zero displacement at the onset of the free motion.

3.2. Non-ideal inputs and problem of determining onset of free motion

The identification method, as indicated above, is based upon the initial condition response of the dynamical system, with $x(0) = 0$ to remove the spurious α_i problem. There are several ways that one might approach measuring such an initial condition response. An ideal impulse response satisfies the initial condition requirements, but cannot be achieved in an experiment. We have chosen to use a non-ideal impulsive excitation and to extract the impulse response, as described below. Another technique to produce this $x(0) = 0$ free response might be to excite the system sinusoidally and then remove the excitation once steady state has been achieved. Yet, another approach to generating the impulse response would be to deconvolve the two signals (force and response) by using a division of their Fourier transforms and inverse transforming the result. However, if the practicalities of implementing these approaches are considered, it can be seen that each approach comes with its own set of difficulties when having to deal with experimental constraints. Results from simulations indicate that the chosen technique, which is essentially a deconvolution of the response and input models, is reasonably robust.

It is expected that the response to non-ideal impulsive inputs, such as one obtained with an impulse hammer, will be close to an ideal initial-velocity response if the impulse lasts a short duration of time. Furthermore, the application of only an initial displacement to generate the response is difficult because of stress relaxation and 'memory' exhibited by the foam. The impulse response of the system needs to be recovered from the available response to non-ideal inputs, by means of a deconvolution technique. It is possible to carry out this process analytically if the input is modelled using some standard (and convenient) functions, such as complex exponentials. Note that the force needs to be sufficiently small, so as to keep the system response linear.

3.2.1. Modified equations for non-ideal impulsive input

Consider an external 'impulsive' force $f(t)$ that lasts for a duration of $t = t_0$ s. It is assumed here that $f(t)$, for $0 \leqslant t \leqslant t_0$, can be expressed as a sum of R complex exponentials. Then the equation of motion for the system is

$$m\ddot{x} + c\dot{x} + kx - k\int_0^t \sum_{i=1}^{N} a_i e^{-\alpha_i(t-\tau)} x(\tau)\,d\tau = f(t). \tag{19}$$

The forcing function $f(t)$ is

$$f(t) = \begin{cases} \sum_{r=1}^{R} F_r e^{\mu_r t} & \text{for } 0 \leqslant t \leqslant t_0, \\ 0 & \text{otherwise} \end{cases} \tag{20}$$

and the initial conditions are $x_0 = 0$ and $\dot{x}_0 = 0$. Let $h(t)$ represent the impulse-response of the system. Then, the system response $x(t)$ is given by the convolution of $h(t)$ with the force $f(t)$ ($x(t) = h(t) \bigstar f(t)$, where $\bigstar$ denotes convolution). Following the notation used for the free-response, let the impulse response be expressed as a sum of $N + 2$ exponentials:

$$h(t) = \sum_{j=1}^{N+2} C_j e^{p_j t}, \tag{21}$$

where $\sum_j C_j = 0$. Convolving the expressions for $h(t)$ and $f(t)$ in Eqs. (21) and (20), respectively, the response $x(t)$ becomes

$$x(t) = \begin{cases} 0 & \text{for } t < 0, \\ \sum_{r=1}^{R} F_r \left(\sum_{j=1}^{N+2} \dfrac{C_j}{\mu_r - p_j} \right) e^{\mu_r t} & \\ - \sum_{j=1}^{N+2} C_j \left(\sum_{r=1}^{R} \dfrac{F_r}{\mu_r - p_j} \right) e^{p_j t} & \text{for } 0 \leqslant t \leqslant t_0, \\ \sum_{j=1}^{N+2} C_j \left\{ \sum_{r=1}^{R} F_r \left(\dfrac{e^{(\mu_r - p_j) t_0} - 1}{\mu_r - p_j} \right) \right\} e^{p_j t} & \text{for } t > t_0. \end{cases} \tag{22}$$

Clearly, given the forcing function in Eq. (20), the residues C_j of the impulse response can be recovered from the measured values of $x(t)$, by using the expression for $x(t)$ for $t > t_0$. Hence, the system identification procedure would proceed by fitting a sum of complex exponentials to the response data for $t > t_0$ (by using Prony's method), using Eq. (22) to calculate the coefficients C_j from the residues of the response, and finally using the C_j and p_j in the second and third steps of the identification procedure to estimate the material parameters.

It can be shown from Eq. (22) that displacement $x(t)$, velocity $\dot{x}(t)$ and acceleration $\ddot{x}(t)$ are continuous at time $t = t_0$. However, the slope of the acceleration response has a jump discontinuity of magnitude $\sum_r F_r \mu_r e^{\mu_r t_0} \sum_j C_j p_j$, at $t = t_0$. This indicates that the acceleration undergoes a sharp change in magnitude at $t = t_0$, at the onset of the free motion. The force imparted by the impact hammer can often be modelled approximately as a half-sine pulse. In that case, the forcing function can be expressed as $f(t) = (K\pi/2t_0) \sin(\pi t/t_0)$, where K is the 'strength' of the input (area under $f(t)$ versus t curve), and the free response is given by

$$x(t) = K \sum_{j=1}^{N+2} C_j \left\{ \frac{1 + e^{-p_j t_0}}{2(1 + (p_j^2 t_0^2/\pi^2))} \right\} e^{p_j t}. \tag{23}$$

The response approaches $Kh(t)$, as $t_0 \to 0$. Hence, for small t_0, $x(t)$, $t \geqslant t_0$, can be assumed to be the impulse response $h(t)$ of the system for system identification purposes. Note that only the relative magnitudes of C_j are needed in the identification procedure and, therefore, the factor of K is irrelevant.

The time t_0 needs to be determined accurately. If the estimated value $\hat{t}_0$ is greater than t_0, some fast decaying terms may not be modelled. If $\hat{t}_0 < t_0$, then two problems arise: (1) the transition from part of the motion when force is active ($\hat{t}_0 < t < t_0$) to the free motion ($t > t_0$) introduces high frequencies into the signal, leading to spurious high-frequency pole clusters in the estimation process (stage 1); and (2) the excitation $f(t)$ contributes directly to the response for $\hat{t}_0 < t < t_0$ and, therefore, a different solution form consisting of a sum of $R + N + 2$ exponentials is required for this portion of the response. Consequently, the error in the location of t_0 must be minimized which requires a high sampling frequency.

3.3. Measurement noise

Measurement noise makes the estimates of residues and system poles (and hence the estimates of frequency and damping components) inaccurate, both in terms of variance and bias. In this section, modifications to the methodology that improve the accuracy of estimation of poles and residues are presented. First, the problem of estimation of poles will be addressed. In Prony's method, where the response data is modelled as a sum of complex exponentials, the poles are estimated by first using a forward prediction model to estimate the coefficients of a polynomial and then finding the zeros of this polynomial. Several different modifications to this basic algorithm have been suggested over the past few years to overcome the problems arising due to noise. Significant among these techniques are: use of high prediction orders [16], use of both forward and backward linear prediction polynomial zeros, singular value decomposition (SVD) based methods [16], and some non-linear schemes [19,20].

3.3.1. Higher model orders and backward prediction

The estimation bias can be reduced by choosing a linear prediction order much higher than the number of exponentials actually present in the signal [21]. It has been observed that if models of several different orders are fitted to the data, the signal poles change very little at high model orders [22,23]. However, the extraneous poles, which in effect attempt to model the noise, change significantly as the model order is changed. Thus, the pole plots in the complex z-domain, resulting from several different order estimations, contain clusters that correspond to the signal poles. As the model order increases, the positions of the clusters approach the pole positions of the noise free signal.

Selection of very high model orders is problematic because of the small amount of data available for estimation, and numerical errors introduced by root solving. As the sampling rate increases, the signal poles all migrate towards the unit circle, which is the region typically occupied by the noise poles. This makes it difficult to identify whether a pole is a signal pole or a noise pole. The issues related to sampling rate selection are discussed in Section 3.4. The problem is illustrated in Fig. 2(a), which shows the poles of a simulated response ($N = 2$) corrupted by a zero-mean, stationary, Gaussian distributed, band-limited noise signal, yielding a 50 dB signal-to-noise ratio (SNR), calculated over the first 2 s of the signal. The noise is band-limited to $0.4 \times F_s$, where $F_s = 256$ Hz is the sampling frequency for the simulations. A fourth order Butterworth filter was used to band-limit the white noise. Model orders of 20–80 were used for the estimation of the system poles. Good clustering behavior is observed, but the true locations are obscured by the presence of too many extraneous poles.

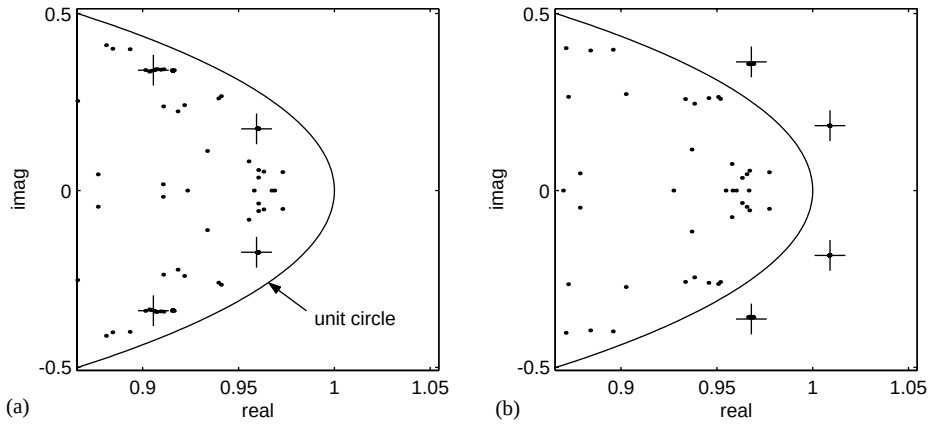

Fig. 2. Pole positions in the complex z-plane for model orders of 20–80. (a) Forward prediction, (b) backward prediction. '·' denotes a pole estimate, '+' denotes the true location of a pole. SNR = 50 dB.

A clearer picture is obtained by applying the estimation procedure to the time-reversed data. Since the system under investigation is stable, the poles of the time-reversed response data appear outside the unit circle, at positions reciprocal to those obtained from the forward prediction on the original sequence. The argument is that the statistics of the broadband stationary random process change little if the process is time reversed. Hence, the extraneous noise-poles tend to remain inside the unit circle. While this is not strictly true for band-limited noise, the extra poles corresponding to the Butterworth filter (used for generating the band-limited structure for the noise) are often difficult to observe. This issue is addressed in Section 3.3.2. Hence for the chosen model orders, the poles of the band-limited noise also remain inside the unit circle. This greatly facilitates locating the position of genuine poles, especially when the clustering of the poles from different model orders is not very good. The results of simulation with time-reversed data, for the same system and model orders, are shown in Fig. 2(b). The locations of genuine poles are clearly identifiable from their clusters, although the clustering itself is poorer for the weaker mode, which in this case is the higher-frequency mode. The estimates of the pole-locations represent the centers of the corresponding clusters.

Further improvement in the estimates of genuine pole locations can be achieved by recording several sets of responses obtained under identical experimental conditions, subjecting them to the estimation procedure with the modifications described above, and superposing the results. This can be done provided that it is possible to repeat the experiments with a high degree of accuracy.

To summarize, good estimates of system poles locations can be obtained by using different but high model orders on the time-reversed data sequence. The true poles are identified by their good clustering behavior. The estimates of pole locations, from individual time series, can then be averaged over several realizations of the system response. It may be noted that the model orders for Prony's series cannot be chosen to be arbitrarily high. Depending upon the level of noise contamination and the length of available response data, there exists an upper limit on the choice of model orders, beyond which the variance of estimation actually increases. Generally, a model order of one-tenth to one-fourth of the total number of data points is considered good for reliable

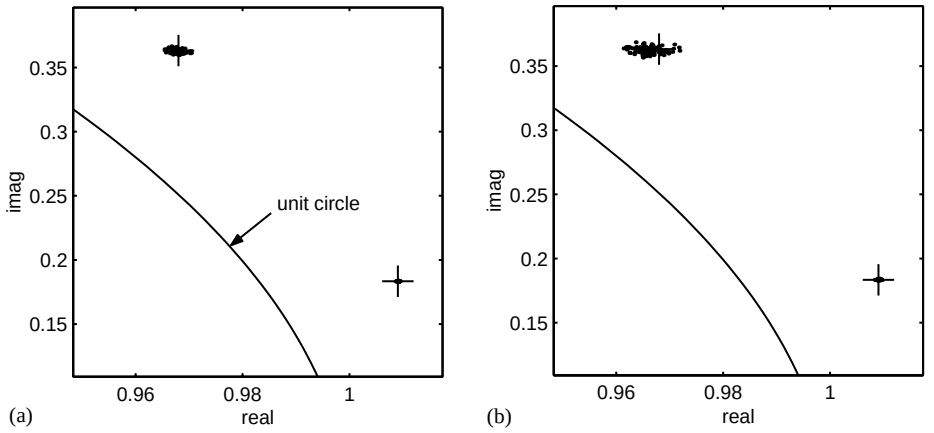

Fig. 3. System poles for time-reversed data for two different SNRs: (a) 60 dB, (b) 50 dB, for 100 independent realizations. '·' denotes a pole estimate, '+' denotes the true location of a pole.

estimation. The method, as presented above, was used for estimation of pole locations for the present work.

The above technique was applied to the simulated response of a system with a two-term relaxation kernel ($N = 2$). The true locations of the four system poles and their estimates for 100 realizations of response, for SNRs of 50 and 60 dB of noise, are shown in Fig. 3. The indicated values of SNRs were their average values across the first 2 s of the time histories. The number of terms ($N + 2$) was determined by observing the number of pole clusters outside the unit circle. The influence of the noise is clear in the increased variance of the pole position estimates in the case of 50 dB SNR. This is particularly noticeable for the second (higher frequency) component of the response.

3.3.2. *Filtering*

An obvious strategy to improve the SNR would be to low-pass filter the data. Here, zero-phase filtering is required since any phase distortion caused by the filter would have an undesirable effect on the identification scheme, which is performed in the time domain. For zero-phase filtering, the signal is first low-pass filtered by using a suitable filter, the filtered data is time reversed and passed again through the same filter, and then time reversed once more [24]. However, the use of filtering has the disadvantage that it imposes additional structure on the data. The set of poles arising from stage 2 of the Prony series will thus include contributions from the filter as well as from the signal and the noise. In the presence of noise, the filter poles generally require high prediction orders for their detection. At low model orders, the presence of the filter poles results in bias in the estimates of the signal poles. This is illustrated in Figs. 4(a) and (b) for a system with $N = 2$. The filter used was a fourth order Butterworth filter with cut-off frequency of 20 Hz. The poles of the filter are not isolated even at model orders as high as 80 for the data length of 256 points. This can be observed in Fig. 4(c). The filtered data contains both the components directly related to the poles of the Butterworth filter as well as their reciprocals, because of the zero-phase filtering process,

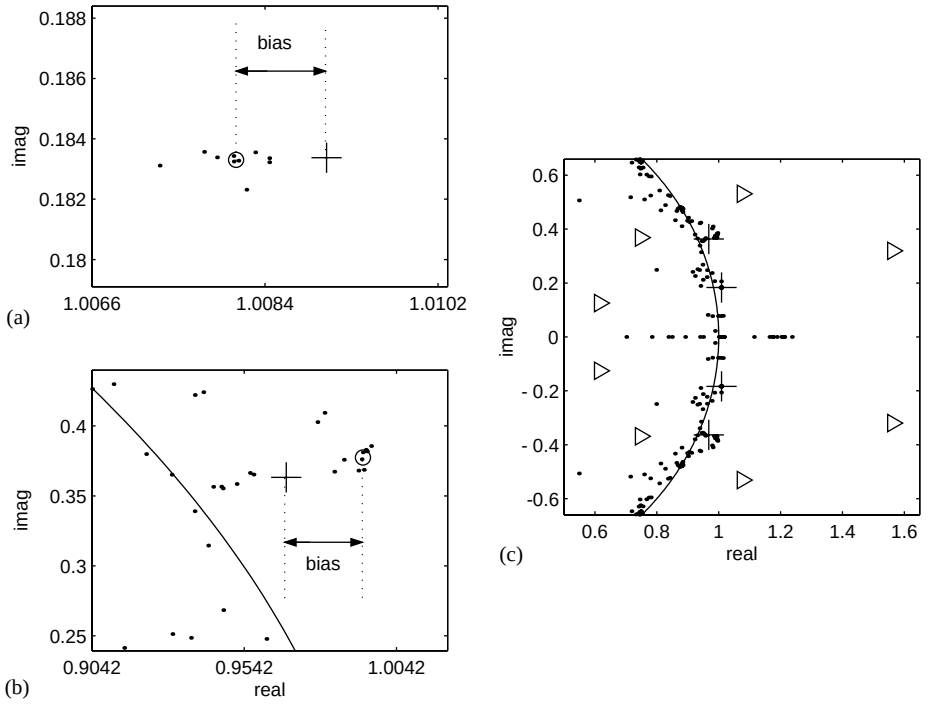

Fig. 4. Problems with use of low-pass filtering. ((a), (b)) Bias in the estimation of system poles caused by zero-phase filtering with a fourth order Butterworth filter. '○' denotes location of a predicted pole. '+' denotes a true location and '·' denotes a pole estimate. (c) Failure in locating filter poles. '▷' denotes a filter pole. Model orders of 20–80 are used for estimation on time-reversed data. SNR = 60 dB.

and the components due to the system's original poles. Thus filtering was not found to be useful in improving the estimation of the system poles.

3.3.3. *Estimation of residues in presence of noise*

Estimation of residues in presence of noise is achieved through a least-squares technique, in the last step of Prony's method. Since the system response has the form given by Eq. (9), the mth sample of the response data $\{x_m\}$ can be written as

$$x_m = \sum_{j=1}^{N+2} C_j (X_j)^m, \quad m = 0, 1, \ldots, (M-1), \tag{24}$$

where M is the number of samples in response sequence $\{x_m\}$ and X_j are the system poles which are related to the eigenvalues p_j by $X_j = \exp(p_j/F_s)$. In a noise-free situation, the first $N+2$ samples of $\{x_m\}$ can be used to set up a linear set of $N+2$ equations, which can be solved for the $N+2$ unknowns C_j. In the presence of noise, more samples of $\{x_m\}$ can be utilized to obtain a least-squares solution for C_j. The least-squares problem can be put in the form

$$\mathbf{VC} = [x]_{\hat{M}}, \tag{25}$$

where $\mathbf{V}$ is a Vandermonde matrix:

$$\mathbf{V} = \begin{bmatrix} 1 & 1 & \dots & 1 \\ \hat{X}_1 & \hat{X}_2 & \dots & \hat{X}_{N+2} \\ \vdots & \vdots & \vdots & \vdots \\ \hat{X}_1^{\hat{M}-1} & \hat{X}_2^{\hat{M}-1} & \dots & \hat{X}_{N+2}^{\hat{M}-1} \end{bmatrix}, \tag{26}$$

$\mathbf{C} = [C_1, C_2, \dots, C_{N+2}]^{\mathrm{T}}$, $[x]_{\hat{M}} = [x_0, x_1, \dots, x_{\hat{M}-1}]^{\mathrm{T}}$, and $(N+2) \leqslant \hat{M} \leqslant M$. Note that the X_i's have been replaced by their estimated values, $\hat{X}_i$, from the first two stages of Prony series modelling. The genuine poles locations are identified by good clustering behavior. Since the response decays with time, the SNR is poorer in the latter part of the signal. This puts an upper limit on the number of data samples that can be utilized for least-square formulation. Higher rows of $\mathbf{V}$ are also subject to larger errors than earlier rows because the estimates of X_i are raised to higher powers [25]. Specifically, if the estimate $\hat{X}_j$ of a pole X_j has an error ε_{X_j}, i.e., $\hat{X}_j = X_j + \varepsilon_{X_j}$, then $\hat{X}_j^n \approx X_j^n + n\varepsilon_{X_j} X_j^{(n-1)}$ in the $(n+1)$th row.

For the system and noise levels considered earlier in the section on estimation of poles, the corresponding residues were also calculated by using the least-squares solution of Eq. (25). The true values and the estimates of the p_j and C_j are shown in Figs. 5 and 6, respectively.

3.3.4. *Presence of components that are difficult to detect*

The model of viscoelasticity, with the relaxation kernel expressed as a sum of exponentials, may contain a large number of time constants. The modelling of the response of the system can always be improved by adding more terms to the relaxation kernel. However, not all components can be detected by a single experiment such as the one considered here. The cases in which the detectability of a mode is hindered, because of presence of noise, are when: (1) there is a small residue C_j associated with the mode: the mode is 'weak' and is difficult to distinguish from the noise floor; (2) there is a very slowly decaying non-oscillatory mode: over the span of

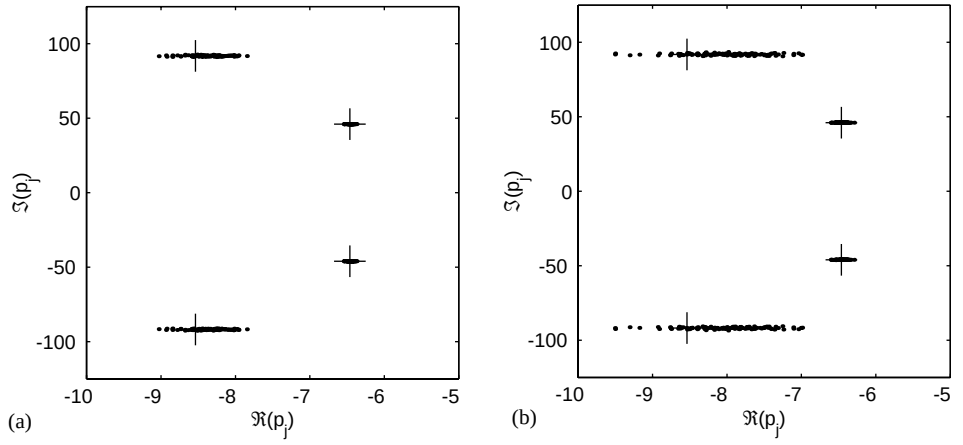

Fig. 5. System eigenvalue estimates for two different SNRs: (a) 60 dB, (b) 50 dB, for 100 independent realizations, for a system with $N = 2$. '·' denotes a pole estimate, '+' denotes the true location of a pole.

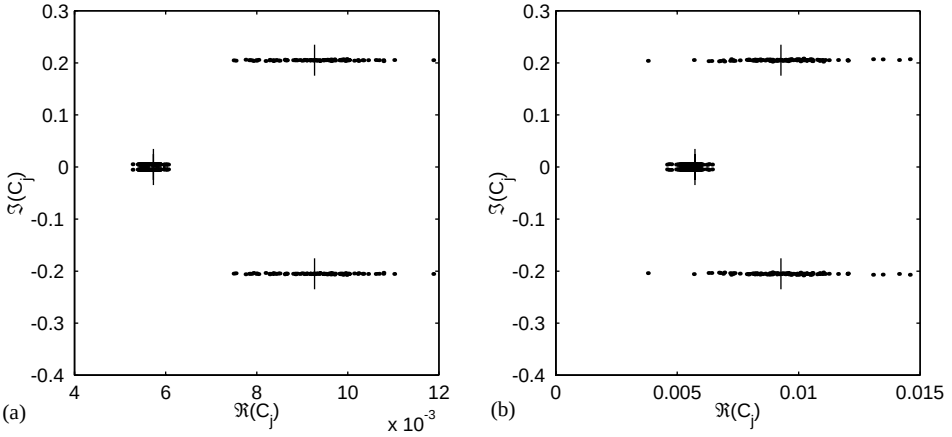

Fig. 6. Residue estimates for two different SNRs: (a) 60 dB, (b) 50 dB, for 100 independent realizations, for a system with $N = 2$. '·' denotes a pole estimate, '+' denotes the true location of a pole.

measurement time, the mode response appears almost as a constant, and hence is a very small component in the acceleration response; (3) there are very fast decaying modes: if the real part of exponent p_j is large, the corresponding mode decays very fast, and thus, for a particular choice of sampling frequency F_s, the mode may be missed for want of a sufficient number of data points to estimate the two unknowns associated with each fast-decaying exponential; and (4) there are closely spaced poles.

These special cases of values of C_j and p_j can be traced to conditions on the values of the system parameters: c, k, a_i and α_i. Here the case of interest is the dependence of the C_j and p_j on the viscoelastic parameters a_i and α_i, since, in the experimental situation, c and k have values close to those of a second order system model with no viscoelastic components. For the case of $N = 1$, the relationships are illustrated in Fig. 7. $\gamma = a/\alpha$ has been chosen as a parameter for analysis, along with α, since γ indicates the stability and damping of the non-oscillatory mode more clearly than the parameter a, for a system with $N = 1$. Specifically, the decay-rate of the non-oscillatory mode of the response reduces as $\gamma \to 1$, and the system is unstable for $\gamma > 1$. As noted in Ref. [26], $\gamma > 1$ renders the model physically meaningless, since it corresponds to the existence of negative stresses. Only the region $\gamma > 0.6$ is shown, since for smaller values of γ, the features are quite regular.

The change in the nature of the roots (p_j), as a function of α and γ can be observed from Fig. 7. The real and imaginary components of p_j are shown separately, while only the magnitudes of the residues C_j are shown. There exists a thin region of values of α and γ for which all the exponents, p_j, are real. The regions of small values of $-\Re(p_1)$, marked by pale shades in Fig. 7(a), represent a combination of parameters for which the non-oscillatory mode decays very slowly. Regions of very high values of $-\Re(p_j)$ are marked by darker shades in Figs. 7(a)–(c), which represent parameter regions where the modes decay very quickly. Similarly, regions of small value of residues, the case of a weak mode, can also be observed in Fig. 7(g) where $\gamma < 0.82$ and $\alpha > 100$. All these regions represent combinations of a and α for which it is generally difficult to identify the three modes, especially the non-oscillatory mode.

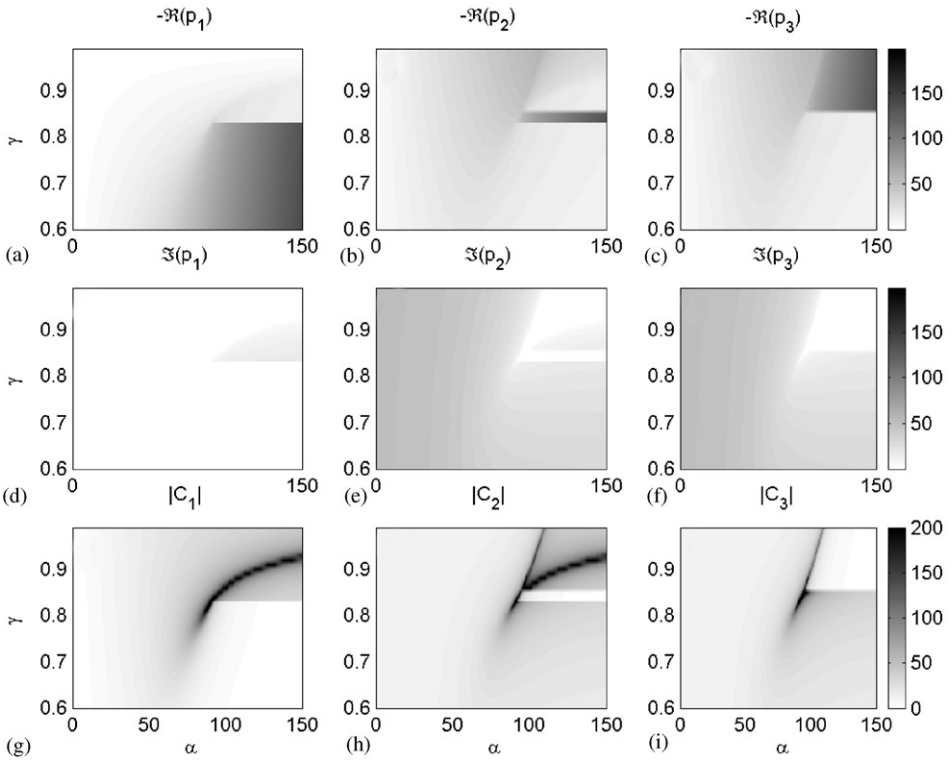

Fig. 7. Dependence of the p_j and C_j on $\gamma = a/\alpha$ and α. (a)–(c): $-\Re(p_j)$, (d)–(f): $\Im(p_j)$, (g)–(i): $|C_j|$.

3.3.5. Other techniques for estimation of signal poles and residues

In this section, some of the popular approaches that were not utilized for the present work, are briefly discussed. The first of these is the method of 'singular value decomposition' (SVD) [27,28]. The SVD procedure can provide an improvement if the singular values associated with the true exponentials are easily distinguishable from those of noise. Then, a 'reduced rank approximation' to the data matrix may be formed by removing the singular values corresponding to noise. This would effectively enhance the SNR of the signal. The number of significant singular values represents the correct model order. If a clear distinction cannot be made between the singular values due to the true exponentials and those due to the noise, such as in the case of weak exponentials in the signal, the method may not provide any improvement.

If the response time series contains modes with time constants of disparate orders, data segmentation can provide significant improvement. The data may be collected at a high sampling frequency. Then the portion of the data where fast decaying components are present (mostly in the beginning of the transient response data) may be segmented out and subjected to the process of pole estimation. The remaining data can be downsampled to a lower sampling frequency and used for further analysis. This can potentially reduce the computation time, especially if the time

series is very long. In a related method, called the 'moving window' approach, data is segmented into several, possibly overlapping, pieces, and Prony's method, with high order forward and backward prediction, is applied to each segment [29]. The signal poles are picked out based on the assumption that they are consistent from one window to another, while the noise-related poles change locations greatly.

Several other methods have also been suggested for estimating the exponents and residues of a Prony series representation of the time series. Some of these are basically similar to Prony's method [13,17,18,30], while others are only empirical techniques [31,32]. Carrot and Verney [13] used a pole-zero (ARMA) model for the relaxation modulus. The authors proposed a method for picking out the correct model orders and 'genuine roots' (system zeros and poles) based on the idea that the extra zeros and poles ('artificial roots'), that are generated if model orders are over-estimated, appear as pairs of very close complex numbers called Froissart doublets. By observing this characteristic over several model orders, all the genuine zeros and poles could be identified, and thus the correct model order also determined.

A 'domain of influence' method was described by Gant and Bower [31] for fitting a sum of exponentials (Prony series) to the response data for viscoelastic materials. The method was based on the idea that an exponential mode has noticeable influence over only a finite scale of time, and that a particular mode can be fitted to a portion of the stress–relaxation curve. The time scale was divided on a decade-scale, and over each decade the dominant time constant was evaluated by observing the change of instantaneous modulus. While the method was shown to generate good curve-fits to test data, no mathematical basis was put forward to explain the rationale behind the adopted approach. A related approach was used by Park and Schapery [32] for finding the time constants in the relaxation modulus of a linear viscoelastic system. The poles corresponding to the modulus were estimated by observing the peaks in the magnitude of the complex modulus function, when plotted on a logarithmic frequency scale.

It may also be noted that the problem of simultaneous determination of both the residues C_j and the poles X_j, based on direct least-squares minimization of the error between the measured response samples and the model x_n, is a highly non-linear and difficult estimation problem. Techniques have been suggested to this effect, such as the method of steepest descent and iterative prefiltering (Steiglitz–Mcbride method) [20]. However, these methods are computationally expensive and exhibit convergence problems [16]. An iterative pole-by-pole estimation method, based on the iterative prefiltering technique, was suggested by Ramalingam et al. [19]. The method is shown to have better convergence properties when compared to the parent algorithm, especially when a large number of signal components (poles) are present.

For specific problems, each one of these approaches has been shown in the literature to yield excellent results. However, there does not seem to be clear evidence that any of these will perform any better than the approach adopted for the research presented in this work. In the presence of significant measurement noise, or for particular cases of nature of response considered in Section 3.3.4, each one of these methods is susceptible to producing poor estimates. Moreover, many of these approaches are fundamentally similar to the approach considered here, as discussed above. Furthermore, the approach considered for the present work allows for easy and direct evaluation of the effect of noise and uncertainties. The technique was found to be numerically stable even for very high model orders, and does not suffer from convergence problems which may be an issue with the iterative schemes.

3.4. Choice of sampling frequency

The sampling frequency for data acquisition needs to be sufficiently high to capture fast decaying modes, as well as to accurately determine the location of onset of the free motion. Too high a sampling frequency, however, would mean a large number of data points for the measured response and hence large computation times. The most significant effect of choosing a high sampling frequency is on the pole estimation in the presence of measurement noise. It may be recalled that the poles X_j are related to the eigenvalues p_j by $X_j = \exp(p_j/F_s)$, where F_s is the sampling frequency in Hz. Thus a high sampling frequency pushes the poles of the system closer to the unit circle. It also increases the error sensitivity for estimation of p_j, since, to the first order, the approximation error in estimation of the eigenvalues is related to the error in estimation of the poles by

$$\Delta p_j = F_s \frac{\Delta X_j}{X_j}. \tag{27}$$

For large values of F_s, $X_j \approx 1$. This makes the error in p_j approximately F_s times the error in X_j. Thus at higher sampling frequencies, the estimation of pole locations needs to be more accurate.

Simulations revealed that for the levels of noise actually present in the experimental data, the accuracy of estimation was not much affected by the choice of sampling frequency so long as no fast decaying components were lost at the lower sampling frequency, and model orders (M) were sufficiently large so that more than one-tenth of the period of all the modes present in the signal were spanned by M/F_s, the model 'length' in seconds. The model orders for observing pole clusters, thus, have to be chosen higher for higher sampling frequencies. This can be done as long as the numerical implementation of the method remains stable and accurate.

3.5. Problem of dry friction

Dry friction can arise in the system in two different ways, one internal to the viscoelastic substance arising from interaction of rubbing surfaces [33], and the other arising in the experimental setup supporting the foam-mass system. The effect of friction on the system response depends on the dynamic model used to describe the friction forces. If a Coulomb friction model is chosen, the effect of external dry friction on the system can be described fairly accurately by incorporating the dry friction term in the forcing function $f(t)$ of the dynamic system being considered here [34]. The appropriate equation of motion is then given by Eq. (7) with non-zero $f(t)$.

For $\dot{x} \neq 0$, the forcing function can be modelled as: $f(t) = -f_0 \operatorname{sgn}(\dot{x})$, where f_0 is a constant representing the kinetic friction force. The equilibrium position x^* is not known in this case, but it satisfies the constraint $|x^*| \leqslant x_s$ [35], where $x_s = f_s/k(1 - \sum_{i=1}^{N} a_i/\alpha_i)$ and f_s is the maximum static friction force. For $\dot{x} \neq 0$, Eq. (7) is piecewise solvable and can be written as

$$m\ddot{x} + c\dot{x} + kx - k\int_0^t \sum_{i=1}^{N} a_i e^{-\alpha_i(t-\tau)} x(\tau)\,d\tau = -f_0, \quad \dot{x} > 0, \tag{28a}$$

$$m\ddot{x} + c\dot{x} + kx - k\int_0^t \sum_{i=1}^{N} a_i e^{-\alpha_i(t-\tau)} x(\tau)\,d\tau = f_0, \quad \dot{x} < 0. \tag{28b}$$

In this case, the response $x(t)$ cannot be expressed as a sum of $N+2$ exponentials. Since the equation changes in every half-cycle (where a *half-cycle* is any continuous piece of motion during which the velocity does not change sign), the corresponding solution is also expected to be different. It can be shown that the solution during ith half-cycle is expressible in the form

$$x(t) = K_i + \sum_{j=1}^{N+2} C_j^i e^{p_j t}, \tag{29}$$

where K_i and the coefficients C_j^i are constants which are different for every half-cycle. Since acceleration data is used for estimation, the information of the constant part K is not directly available from the measured time series. A closed-form solution for the free response of the system and an analytical procedure, for calculating friction and the system parameters in the presence of dry friction, have been presented by Singh et al. [34].

The system identification procedure developed in Ref. [34] is based on the availability of residues and eigenvalues for the acceleration response. The data for each half-cycle needs to be modelled independently as a sum of a constant and $N+2$ exponentials, as described by Eq. (29). In practice, the estimation of these coefficients using Prony's method directly on response data, as described in Section 1.3, is difficult because of limited data-length available in any half-cycle. Some improvement in the estimation of poles can be achieved by combining information from individual half-cycles. Since the eigenvalues p_j are the same for all the half-cycles, the linear prediction equations obtained from individual half-cycles, in the first step of Prony's method, can be grouped together when finding the least-squares solution for coefficients of prediction polynomial. This process leads to a unique set of system poles for the complete data. However, the maximum allowable model order is limited by the size of the data from the shortest half-cycle. Specifically, if the response of a system is represented by $\{x_n\}$, then the system of equations for estimation of the coefficients A_i of the pth order prediction polynomial, in absence of dry friction, obtained in the first step of Prony's method, can be represented as

$$\begin{bmatrix} x_{p-1} & x_{p-2} & \cdots & x_1 & x_0 \\ x_p & x_{p-1} & \cdots & x_2 & x_1 \\ \vdots & \vdots & & \vdots & \vdots \\ x_{N-3} & x_{N-4} & \cdots & x_{N-p-1} & x_{N-p-2} \\ x_{N-2} & x_{N-3} & \cdots & x_{N-p} & x_{N-p-1} \end{bmatrix} \begin{bmatrix} A_1 \\ A_2 \\ \vdots \\ A_{p-1} \\ A_p \end{bmatrix} = - \begin{bmatrix} x_p \\ x_{p+1} \\ \vdots \\ x_{N-2} \\ x_{N-1} \end{bmatrix}, \tag{30}$$

where N is the total data length, and $A_0 = 1$. The system of equations for estimation of A_i in presence of dry friction can be obtained from Eq. (30) above, by removing the rows that have data x_n spanning over two or more different half-cycles.

The residues C_j^i for each half-cycle can be obtained by using Eq. (25), since the exponents p_j are known. The equations of displacement continuity and velocity continuity, at the intersection of two consecutive half-cycles, can be used as additional constraints in this estimation process, and the residues for all the half-cycles can then be estimated simultaneously, in an optimized fashion. More details of this analysis can be found in Ref. [34].

3.6. Propagation of errors in residues and poles to material parameter estimates

In the previous sections, various factors affecting the estimation procedure were studied and modifications to the identification procedure described to deal with the associated problems. The net effect of the errors and uncertainties is to introduce errors in estimation of the exponents p_j and residues C_j. These errors are propagated to the final estimates of the system parameters: c, k, α_i and a_i, in the second and third stages of the identification procedure.

For the case of systems with $N = 1$, an algebraic analysis was carried out to evaluate the effect of small errors in the estimation of C_j and p_j on the final estimates of the system parameters.

The residues C_j and the exponents p_j are assumed to have independent additive errors ε_j and δ_j, respectively, so that the estimates $\hat{C}_j$ and $\hat{p}_j$ can be written as

$$\hat{C}_j = C_j + \varepsilon_j \tag{31}$$

and

$$\hat{p}_j = p_j + \delta_j, \quad j = 1, 2, \ldots, N+2. \tag{32}$$

In the estimation of α, the roots of a quadratic equation ($\beta_{1,2}$) are determined. The two roots are

$$\beta_1 = \alpha, \quad \beta_2 = \beta_{spurious} = \frac{c}{m} + \frac{\dot{x}_0}{x_0}, \tag{33, 34}$$

where $x_0 = \sum_j C_j$ is the true value of the initial displacement, and $\dot{x}_0 = \sum_j C_j p_j$ represents the true value of the initial velocity. By using Eqs. (31) and (32), it is possible to propagate the errors in the C_j and p_j to errors in the roots $\beta_{1,2}$ of α. Their estimated values, denoted $\hat{\beta}_{1,2}$, are related to their true values, to the first order of approximation, by

$$\hat{\beta}_{1,2} = \beta_{1,2}\left(1 - \frac{\Delta x_0}{x_0} \mp \frac{\Delta b}{D}\right) \mp \left(\frac{\Delta g}{D} + \frac{g\Delta x_0}{D x_0}\right), \tag{35}$$

where upper signs correspond to $\hat{\beta}_1$ and the lower signs to $\hat{\beta}_2$. $\Delta x_0 = \sum_j \varepsilon_j$ denotes the error in the estimation of x_0. The quantities Δb, D, g and Δg are related to the errors ε_j and δ_j by the following expressions:

$$\Delta b = -\left(\alpha + \frac{c}{m}\right)\Delta x_0 + x_0 \sum_j \delta_j - \Delta \dot{x}_0, \tag{36}$$

$$D = \dot{x}_0 + x_0\left(-\alpha + \frac{c}{m}\right), \quad g = \left(x_0 \frac{c}{m} + \dot{x}_0\right)\alpha \tag{37, 38}$$

and

$$\begin{aligned}\Delta g = & -x_0\left(\left(\alpha + \frac{c}{m}\right)\sum_j \delta_j + \sum_j p_j \delta_j\right) + \left(\frac{k + c\alpha}{m}\right)\Delta x_0 \\ & + \left(\alpha + \frac{c}{m}\right)\Delta \dot{x}_0 - \dot{x}_0 \sum_j \delta_j + \Delta \ddot{x}_0,\end{aligned} \tag{39}$$

where $\Delta \dot{x}_0 = \sum_j C_j \delta_j + p_j \varepsilon_j$, and $\Delta \ddot{x}_0 = 2\sum_j C_j p_j \delta_j + \sum_j p_j^2 \varepsilon_j$ denote the errors in the estimation of the initial values of the velocity and the acceleration, respectively.

From Eq. (35), it can be deduced that for small values of x_0, the error in estimation of α will be amplified. For impulse tests x_0 will usually be small and hence error-sensitivity is expected to be large. This holds true also for systems with $N > 1$, since the coefficient of the highest order term in Eq. (17) is always x_0. Thus even for small errors in C_j and p_j, there exists the possibility of a large error in estimation of α_i. For impulse tests, the system is known to be initially at rest before the impulse is imparted (i.e., $x_0 = 0$). For this case, the two roots $\hat{\beta}_{1,2}$, to the first order of approximation, are given by

$$\hat{\beta}_1 = \alpha, \quad \hat{\beta}_2 = \hat{\beta}_{spurious} = \frac{c}{m} + \frac{\dot{x}_0 + \Delta\dot{x}_0}{\Delta x_0}. \tag{40, 41}$$

Thus for impulse tests, the genuine root is approximated to its true value, to first order of approximation.

The estimation procedure for other parameters involves solving a set of linear equations, and the errors do not show a similar direct sensitivity to initial conditions. However, the values do depend upon estimated value(s) of α_i. For the case of $N = 1$, these errors are bounded as

$$\Delta c \leqslant m\left(|\Delta\alpha| + \sum_j |\delta_j|\right), \tag{42}$$

$$\Delta k \leqslant m\left\{\left|\left(\alpha - \frac{c}{m}\right)\Delta\alpha\right| + \frac{c}{m}\sum_j |\delta_j| + \sum_j |\delta_j p_j|\right\} \tag{43}$$

and

$$\Delta a \leqslant \frac{k|\Delta\tilde{a}| + |a\Delta k|}{k^2}, \quad \text{where } \Delta\tilde{a} = m\tilde{a}\sum_j \frac{\delta_j + \Delta\alpha}{p_j + \alpha}. \tag{44}$$

The results for the case of two terms ($N = 2$) are qualitatively similar to these results. This error analysis is valid only if the errors δ_j and ε_j are small relative to p_j and C_j. While this is generally true for the experimental conditions considered here, it may not always be correct. Typical examples include cases where the response contains weak exponentials or components which decay either very quickly or very slowly. In these cases, the errors in estimation of the eigenvalues and residues may not be small.

The estimates of C_j and p_j from simulated responses with SNRs = 60 and 50 dB (as reported in Section 3.3) were used for estimation of system parameters. Over 500 different randomly generated combinations of C_j and p_j, within the range of variation of their values for the given noise level, were used for estimation of the parameters. The results (mean values and standard deviations) are shown in Table 1. The standard deviations are shown in parenthesis below their respective mean values. For complex quantities, the standard deviations were calculated separately for the real and the imaginary parts. Good accuracy in estimation is observed. However, the estimation of the coefficients a_i and $\Re(\alpha_i)$ is more sensitive to noise than the estimation of the other parameters.

Table 1
Effect of measurement noise on estimation of C_j, p_j and system parameters

	True values	Estimates SNR = 60 dB	Estimates SNR = 50 dB
$p_{1,2}$	-8.537 ± 91.906i	-8.374 ± 91.847i $(0.240 \pm 0.031$i$)$	-8.028 ± 91.869i $(0.520 \pm 0.590$i$)$
$p_{3,4}$	-6.463 ± 46.021i	-6.457 ± 46.026i $(0.034 \pm 0.031$i$)$	-6.459 ± 46.031i $(0.057 \pm 0.058$i$)$
$C_{1,2}$	0.0057 ± 0.0049i	0.0056 ± 0.0049i $(0.0001 \pm 0.0002$i$)$	0.0055 ± 0.0048i $(0.0003 \pm 0.0004$i$)$
$C_{3,4}$	0.0093 ± 0.2051i	0.0093 ± 0.2051i $(0.0008 \pm 0.0007$i$)$	0.0093 ± 0.2052i $(0.0016 \pm 0.0011$i$)$
$\alpha_{1,2}$	10 ± 90i	9.816 ± 89.953i $(0.265 \pm 0.401$i$)$	9.454 ± 90.031i $(0.567 \pm 0.659$i$)$
$a_{1,2}$	-3 ± 5i	-2.978 ± 4.944i $(0.208 \pm 0.129$i$)$	-3.025 ± 4.796i $(0.357 \pm 0.252$i$)$
c	10	10.031 (0.159)	10.068 (0.297)
k	2500	2497 (13)	2487 (23)
R^2	—	0.9999	0.9998

4. Experimental analysis

In this section, the results of applying the system identification procedure to measured responses of the foam-mass system (shown in Fig. 1) are given, along with the testing procedures necessary to produce repeatable results. The initial tests, that illustrate the application of the system identification procedure to short-duration impulse responses, were conducted with the foam at 55% static pre-compression, which was obtained by using a mass of $m = 1.2$ kg. Tests were then conducted at various compression levels to examine the variation in the model parameters as a function of precompression level. Finally, an analysis of the quasi-static creep behavior is presented.

4.1. Experimental set-up and data-acquisition system

The system was composed of a 3-in foam cube loaded with a mass on the top. The foam cubes were cut from the bolsters of a car seat cushion. A fixture was fabricated, consisting of a rigidly fixed base plate and four vertical guide posts that constrain a metal block to move in the vertical direction. The foam cube is sandwiched between the metal block and the base. A schematic diagram of the experimental set-up is shown in Fig. 1. The foam cube is glued to thin metal plates, which are in turn bolted to the base plate and to the top block to prevent the top block from losing contact with the foam during vibration. Low-friction linear bearings are used to guide the block and minimize the effects of sliding contact points between the top block and the guide posts. Additional mass blocks can be attached to the top of the primary block to increase the level of pre-compression. An instrumented PCB-made piezoelectric hammer (Type no. 086C03) with a rubber tip was used to generate and measure an impulsive input to the foam-mass system.

Four Kistler Type 8303 accelerometers (DC to 40 Hz) were placed on top of the metal block to measure the transient response of the foam-block system with minimum rocking (explained in next section). The accelerometer and force transducer signals were passed through 120 dB/Octave roll-off, analog, anti-aliasing filters, part of a HP3566A data acquisition (16 bit) and spectrum analyzer system. The cut-off frequency of the filters was set to be 0.41 times the sampling rate (F_s). The sampling frequency used was 4096 samples/s. The frequencies present in the transient response of the foam-mass system were typically below 50 Hz, and thus well separated in frequency from any ringing effects induced by the sharp roll-off of the anti-aliasing filter above 1680 Hz. No other filter was used during the data acquisition.

4.2. Testing methodology for short-duration transient tests

Owing to the viscoelastic properties exhibited by the foam, the response of the foam shows dependence on past history of loading and on recovery time allowed between different tests. The behavior is different for loading and unloading paths in a cycle because of hysteresis in the foam [3]. The foam behavior is also dependent on the ambient temperature and humidity. The results are also affected by friction in the bearings of the test rig and by the non-ideal excitations.

1. *Memory of the foam and hysteresis*: A period of 2 days was found to be sufficient for the system to reach equilibrium, both during loading and unloading cycles. Tests were carried out in the loading part of the hysteresis loop. Thus, before every test, the foam block was first left completely unloaded for at least 2 days to recover fully from any residual stresses. Then the foam block was loaded with the required mass and was left for 2 days to settle (creep) to the new equilibrium position, after which the impulse testing was performed.
2. *Rocking motion and friction in bearings*: Unidirectional motion of the system is required for the validity of the model. The foam-mass is constrained to move in a single, vertical direction by the four vertical guide posts. However, small in-plane rotations of the top plate can be caused by non-uniformity in the foam, unequal friction in the four linear bearings, and if the applied impulse is not perfectly centered. Tight fitting bearings reduce the rocking, but at the cost of increased friction. It was desirable to reduce friction. So the bearings were installed to fit loosely around the shafts and a thin lubricant was applied. Rocking effects were monitored by comparing the responses of the four accelerometers placed close to the four edges on top of the metal block. When the four responses were found to be very close, as is the case shown in Fig. 8, they were averaged and the result used in subsequent system identification. Providing an impulse that resulted in negligible rocking motion was difficult and, thus, many impulse responses had to be generated to obtain one which was sufficiently acceptable for further analysis.
3. *Other sources of error*: In order to ensure that non-linear effects were small, the amplitude of input force from the impact hammer was kept sufficiently small. This was ensured by monitoring the maximum displacement following the application of an impulse, and was kept less than 1 cm. Ambient temperature and humidity were also monitored during the tests because they affect the foam behavior. For the tests described below, the temperature and relative humidity varied between 20°C and 25°C, and 35% and 60%, respectively, and thus variations in the response due to variations in temperature and humidity were small.

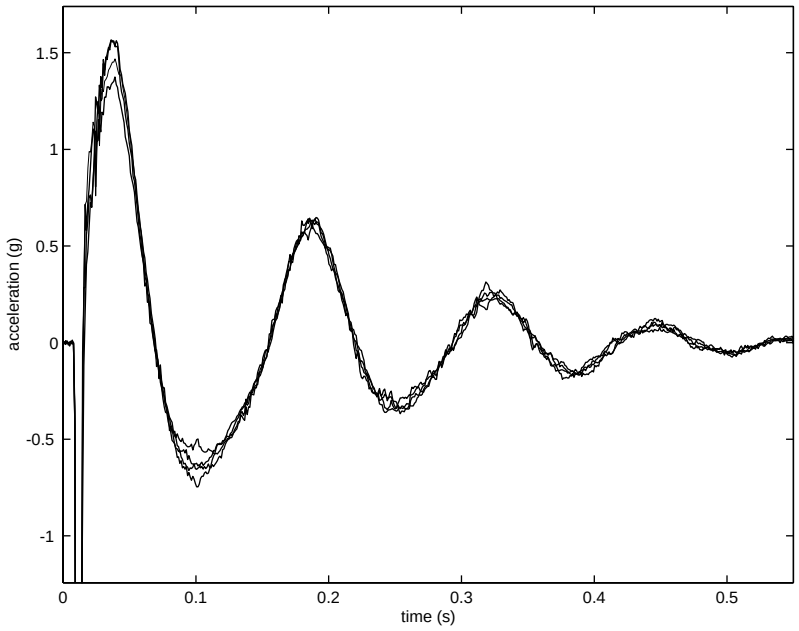

Fig. 8. Four acceleration measurements from the top of the metal block, illustrating the results of a typical test with a low level of rocking.

Repeatability of results was monitored by repeating the tests, including the 4-day unloading and loading sequence. Three to five transient responses were measured in each test, and tests were repeated at least three times. In subsequent plots where error bars are given, these represent the maximum and minimum estimate of the parameter of interest from those 9–15 transient response measurements.

4.3. Analysis of short-duration free response data

4.3.1. Determining t_0 and modelling the input force

A typical input and averaged acceleration response are shown in Fig. 9. The earlier part of the force and response time histories are also shown in Fig. 10, along with a half-sine pulse model of the input force: $f(t) = 121.3 \sin(826.735t - 7.771)$. A much more accurate representation of the input can be constructed by fitting a 12-term Prony series model to the force time history. These models of the input force were used to correct the estimates of the residues in Prony series model, and to convert the free response model to an impulse response model, as described in Section 3.2.

The effects of the hammer tip's impulse response makes it difficult to ascertain the exact time at which the impulsive excitation ends and the free response begins (t_0). However, at this point the acceleration response also undergoes a sharp jump in derivative. Although not obvious from Fig. 10, by using a high sampling frequency (4096 Hz) and expanding the input and response time histories, the location of time t_0 can be accurately determined. Typically, t_0 is of the order of 10 ms.

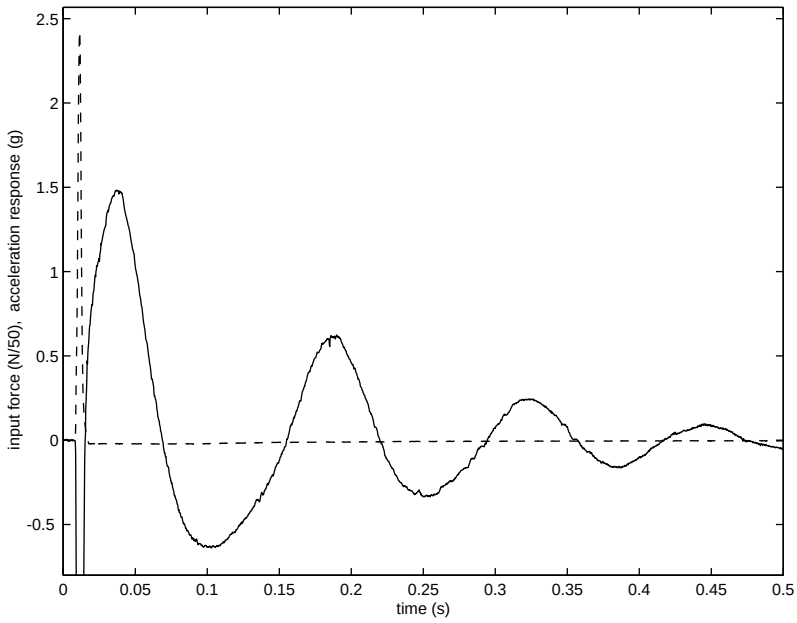

Fig. 9. A representative sample of the input force (dashed line) and acceleration response (solid line) of the system. Response is obtained by averaging the measurements made by using the four accelerometers.

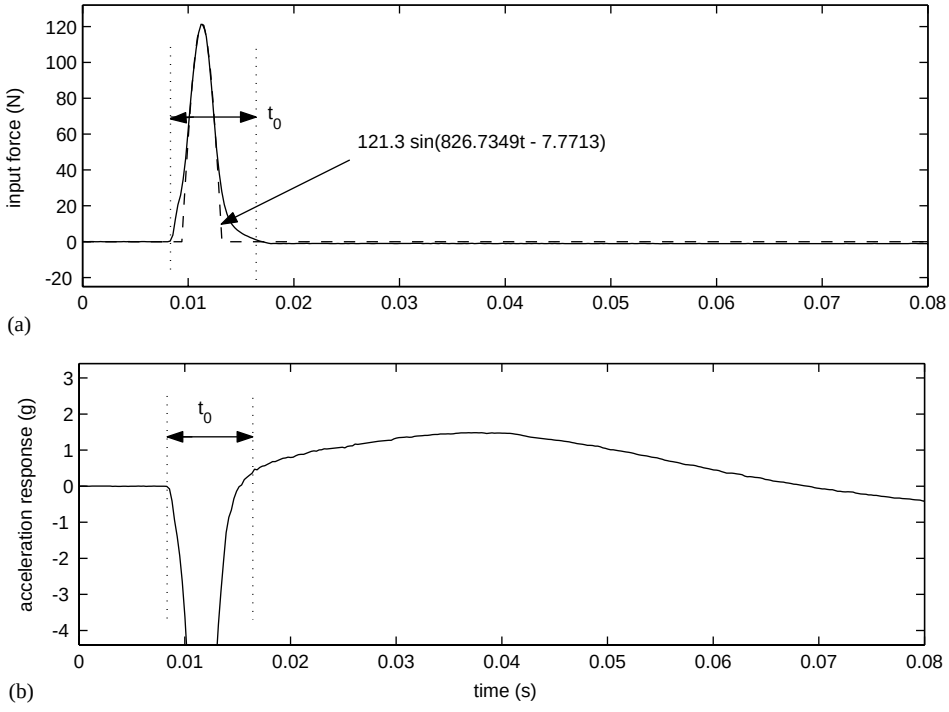

Fig. 10. (a) Input and (b) response plots zoomed around the region of the onset of free motion. Note the sharp change in response at $t = t_0$. The half-sine model of the input is shown by dashed line in (a).

4.3.2. Determination of model order and estimation of C_j and p_j

Two thousand points ($\approx$0.5 s of data) of the free response ($t > t_0$) from a 55% compression test were analyzed. Prony series models, fit to the time reversed signal, of order 150–450 in steps of 25, were estimated and the pole locations plotted to identify clusters. These clusters are shown in Fig. 11. The genuine modes are chosen on the basis of their good pole-clustering behavior. Clusters at high frequencies were also observed for high model orders. These are most likely related to the poles of the anti-aliasing filters that are very close to the unit circle, a result of the very sharp roll-off characteristics of the filters. In these cases, the 'noise pole-clusters' are distinguished from those of the system based on the following two criteria: (1) the generally high frequencies, and (2) the much smaller residues, associated with them. Results from different independent experiments were also compared to pick out the system poles, which are expected to remain fairly stationary in location from test to test.

Typically, two pairs of clusters of complex conjugate poles are observed with significant residues. Good clustering behavior is observed for the lowest-frequency (6.91 Hz) pair of poles, while the clustering is poorer for the second pair of poles located at a frequency of 13.14 Hz. The lowest-frequency component dominates the response (it has the highest residue), while the additional pair of poles provides a 'correction' term to this predominantly single-frequency response. This suggests that the transient behavior of the system is predominantly elastic in nature, with small contribution from the viscoelastic components. An even weaker (smaller amplitude) mode is also discernible from noise floor at a frequency of 19.6 Hz, if an input force of

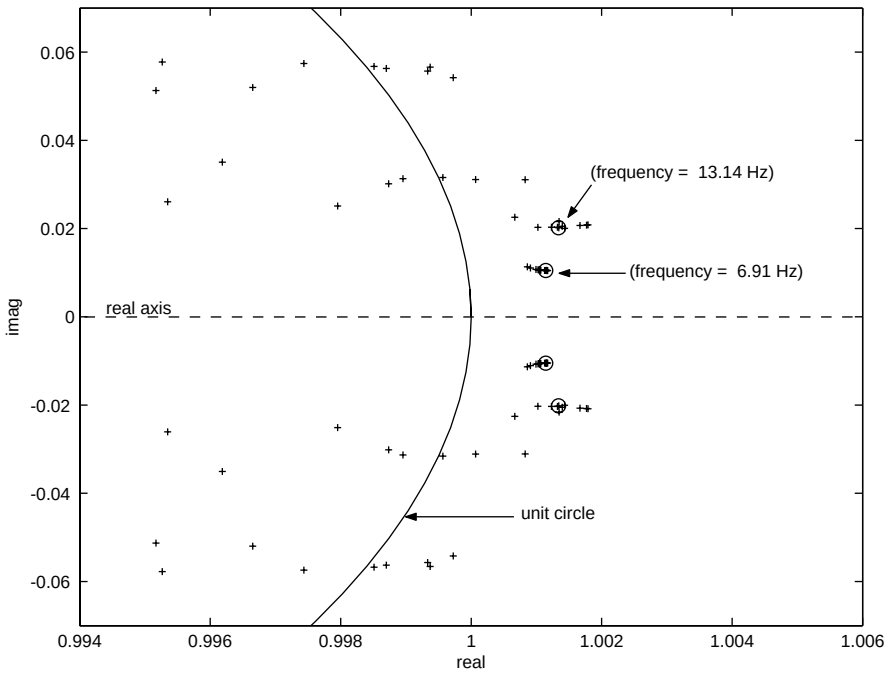

Fig. 11. Pole locations for the time-reversed experimental data, shown by '+'. Model orders of 150–450 are used. The approximate location of a cluster is indicated by '○'. The cluster pair closer to real axis (6.91 Hz) is dominant (higher residue).

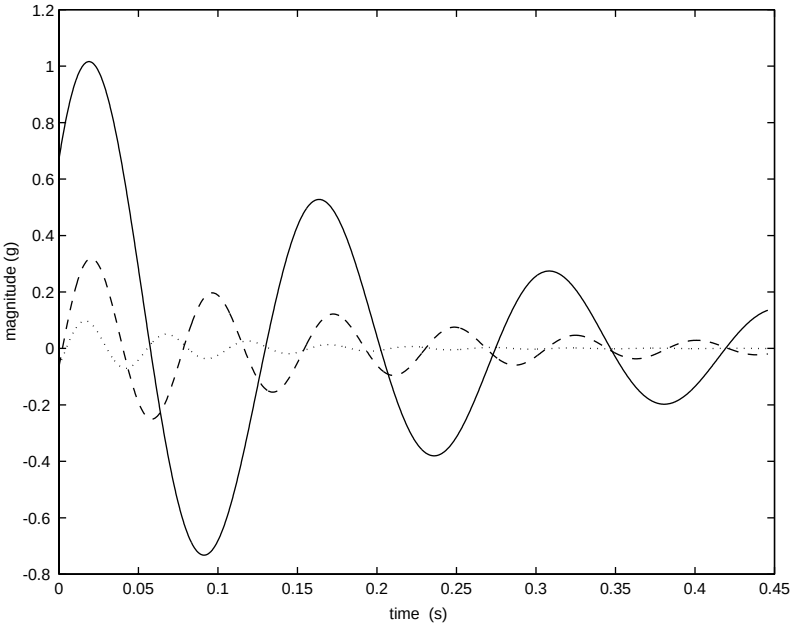

Fig. 12. The three constituting components of the experimental free response, obtained by identifying the three dominant pole-pair clusters. The solid line (—), dashed line (- -), and dotted line (···) represent the first, second and third components, respectively.

slightly higher amplitude is used during the experiment. The individual contributions of the three modes to the acceleration response are shown in Fig. 12. The locations of these 3 pairs of poles are: $X_{1,2} = 0.9988 \pm 0.0105\text{i}$, $X_{3,4} = 0.9983 \pm 0.0201\text{i}$, and $X_{5,6} = 0.9964 \pm 0.0300\text{i}$.

The experimental system response for $t > t_0$ was compared with the modelled responses with one, two and three pairs of complex conjugate poles (see Fig. 13). The case of one pair of poles (the primary frequency component only) represents the non-viscoelastic approximation of the model. As seen, the fit to experimental data with only the main frequency component is poor, thus indicating the significant role of viscoelasticity. The modelled responses with two or three pairs of poles match the experimental data well in the early half of the response, but the agreement is poor in the latter half (see Fig. 13). The two and three mode predictions are very close to each other for most of the time history. For most of the subsequent analysis, the pair $X_{5,6}$ was not included, and the model order was taken to be four, that is, $N = 2$ for the relaxation kernel. Simulations of three mode systems were analyzed using two mode approximations to determine the effect of excluding the third mode. It was found that omission of this weak third mode lead to relatively small errors in the estimation of material parameters, except, perhaps, in that of viscous damping c. This is illustrated in columns three and four of Table 2.

4.4. Higher order models

To examine the possible reasons for poor agreement between the model prediction and the measured response at later times, the response was modelled by using a Prony series with even

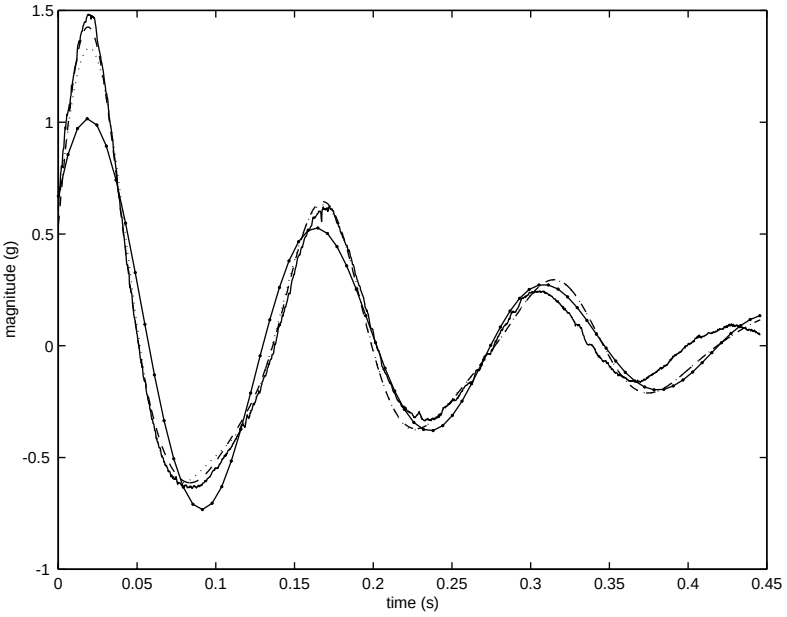

Fig. 13. The measured free response and the response predicted by using 1 pair (solid line with dots), 2 pairs (dotted line) and 3 pairs (dashed line) of pole clusters. The two mode and the three mode predictions are almost the same after about 0.125 s. The experimental data is drawn with solid line.

higher model orders, as high as 800 for a data length of 2000 points. It was found that the pole-clusters corresponding to the system undergo a small 'drift' in location, as model orders are increased from 150 to 800. Typically, for the first two most significant modes, the corresponding pair of pole clusters both change their location twice (see Fig. 14). One possible reason for this drift is the presence of closely located modes in the response, which cannot be resolved into distinct modes by the Prony series modelling. Prony analysis of simulations of responses containing closely located modes in the presence of noise (SNR in the range of 60–100 dB) exhibited the same drifting behavior in clustering as was observed with the experimental data. If the first pair of pole clusters is replaced by three pairs of closely located pole clusters, the second pair is replaced by two pairs of pole clusters, and the resulting six pairs of poles are used for estimation of the residues, a much better fit to the experimental response is obtained, as shown in Fig. 15. The locations of these six pairs of poles are: $X^1_{1,2} = 0.9988 \pm 0.0105\text{i}$, $X^1_{3,4} = 0.9997 \pm 0.0121\text{i}$, $X^1_{5,6} = 0.9982 \pm 0.0098\text{i}$, $X^2_{1,2} = 0.9983 \pm 0.0201\text{i}$, $X^2_{3,4} = 0.9978 \pm 0.0207\text{i}$, and $X^3_{1,2} = 0.9964 \pm 0.0300\text{i}$, where the superscripts denote the closeness of these poles to the original locations. Note that the old clusters have retained their locations, while 3 new pairs of (possible) pole clusters have been added. The inability of Prony's method to resolve such closely space modes with moderately high model orders was verified by numerical simulations. Hence this phenomenon should be investigated further.

Another reason for the drift in the pole locations could be the presence of friction in the system, in which case, the model assumptions for the system response are not valid. In the presence of dry friction, the response is different for each half-cycle [34], and hence the Prony technique should

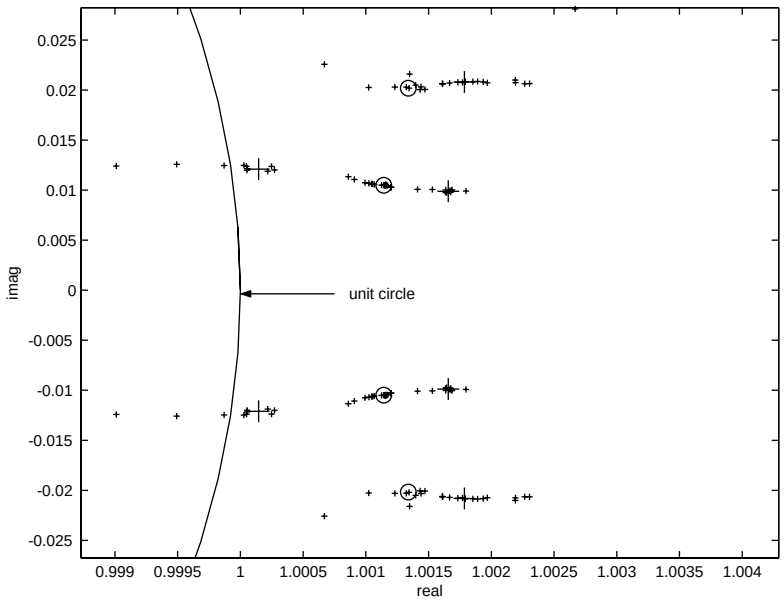

Fig. 14. The drift in the original pole clusters when higher order models (450–800) are used. Original clusters are shown by a '○', while the new *drifted* locations at higher model orders are indicated by a '+'. '+' denotes estimated pole location.

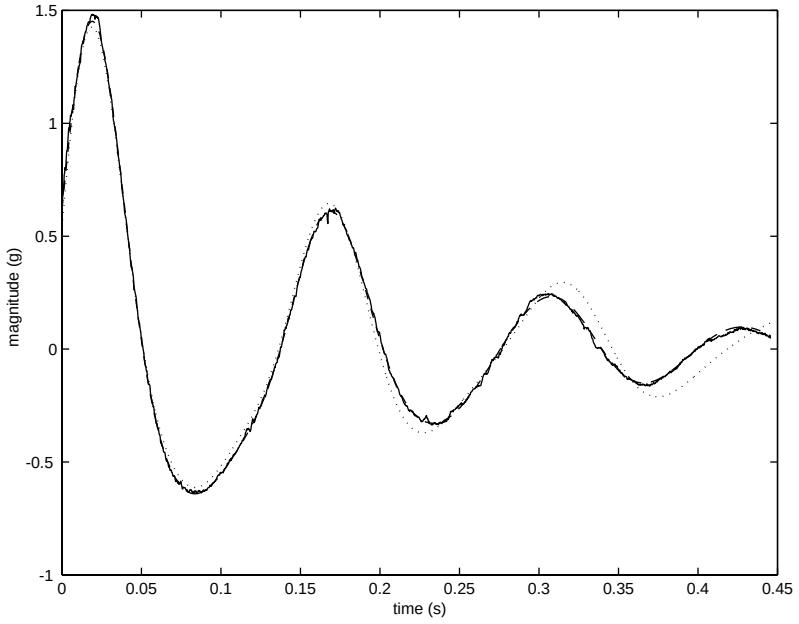

Fig. 15. The measured response (—) and the response of the 3 pole-pair (···) and 6 pole-pair (- - -) models.

not be applied directly. In doing so, the Prony series model will attempt to model the discontinuities within the data at the end of each half-cycle and this may also cause pole locations to shift, as more discontinuities are spanned by the model. So the improvement may just be due to an increase in modelling capability with increased model order.

4.4.1. Conversion of the free response model to an impulse response model

After the exponents and residues for the free motion data were identified, the impulse response coefficients C_j were determined by using Eq. (22). The coefficients F_r and μ_r for the forcing function $f(t)$ were determined by fitting a 12-term Prony series to the input force data for $0<t<t_0$. The residues generated from modelling of the acceleration response after $t = t_0$, and those of the corresponding impulse response (extracted by using Eq. (22)), are shown in the first two rows of Table 2.

The estimates of the system parameters were obtained by using the procedure outlined in Section 2. For $N = 2$, Eq. (13) was solved for three roots of α_i, yielding one real and a complex conjugate pair of roots. The real root was identified as the spurious root related to the initial conditions and this was verified by conducting impact tests with slightly different input force amplitudes. Its value was again verified by using Eq. (18). The complex conjugate pair $\alpha_{1,2}$ was used in step 3 of the identification procedure for estimation of the remaining parameters: c, k, and $a_{1,2}$.

If the free response model for data after $t = t_0$ s, with acceleration integrated twice to give displacement, is assumed to be the true impulse response of the system, the errors in the identified system parameters are usually less than the observed experimental variability (see the 55% compression data in Fig. 17). In doing so, the free response must be traced back to the proper initial conditions for the impulse response, that is, $x_0 = 0$. This can be done by multiplying the residue $\hat{C}_j$ of the free response after $t = t_0$ with a correction factor of $e^{-p_j\hat{t}_0}$, that is $C_j = \hat{C}_j e^{-p_j\hat{t}_0}$, where $\hat{t}_0$ is the time correction required to make $x_0 = \sum_j C_j = 0$, and C_j are the genuine residues to be used. Note that there is no deconvolution involved in this process. The parameter estimates for the two cases (uncorrected and corrected) are shown in columns two and three of Table 2. While this indicates that the free motion, beyond $t = t_0$ can be assumed to be the impulse response of the system without introducing any significant error, the correction was still applied for all the results presented here.

Table 2
Estimation of system parameters with and without residue correction

	Original values Two mode model	Corrected values Two mode model	Corrected values Three mode model
$C_{1,2}$ ($\times 10^{-3}$)	$(-0.24 \pm 3.02\text{i})$	$(-1.91 \pm 8.38\text{i})$	$(-2.01 \pm 8.29\text{i})$
$C_{3,4}$ ($\times 10^{-4}$)	$(0.24 \pm 0.14\text{i})$	$(5.42 \pm 5.70\text{i})$	$(5.47 \pm 5.21\text{i})$
$C_{5,6}$ ($\times 10^{-5}$)	—	—	$(1.24 \pm 0.26\text{i})$
c (Ns/m)	1.09	2.20	0.10
k (N/m)	2871	2799	2832
$\alpha_{1,2}$ (1/s)	$10.35 \pm 80.32\text{i}$	$10.30 \pm 79.79\text{i}$	$10.42 \pm 80.22\text{i}$
$\alpha_{3,4}$ (1/s)	—	—	$14.88 \pm 122.95\text{i}$
$a_{1,2}$ (1/s)	$-6.57 \pm 7.35\text{i}$	$-6.62 \pm 7.06\text{i}$	$-7.25 \pm 6.04\text{i}$
$a_{3,4}$ (1/s)	—	—	$-10.22 \pm 4.22\text{i}$

5. Variation of model parameters with compression level

The experimental methodology presented above was used for estimation of the system parameters at several levels of static compression, ranging from 30% to 60%. For compression levels less than 35%, only one pair of complex-conjugate poles could be distinguished from the noise floor. Thus, the behavior of the system was predicted to be essentially viscously damped in nature, without memory effects, at this compression level. To illustrate the variability in the Prony series parameter estimates, the real and imaginary parts of the p_j and corrected C_j are shown in Fig. 16, along with their corresponding error bars. The estimated values of the system parameters, along with the maximum and minimum estimates of these parameters from different tests, are shown in Fig. 17.

The estimates are based on data from six independent response realizations. The damping and stiffness values estimated from a model without viscoelastic terms are also shown for comparison. Both viscous damping and stiffness tend to increase as compression is increased. The imaginary part of α, which may be called the 'viscoelastic frequency', also increases with increase in compression. No definitive trends could be observed in the real part of α (which represents 'viscoelastic damping'), or in the real and imaginary part of a. These estimates of these three

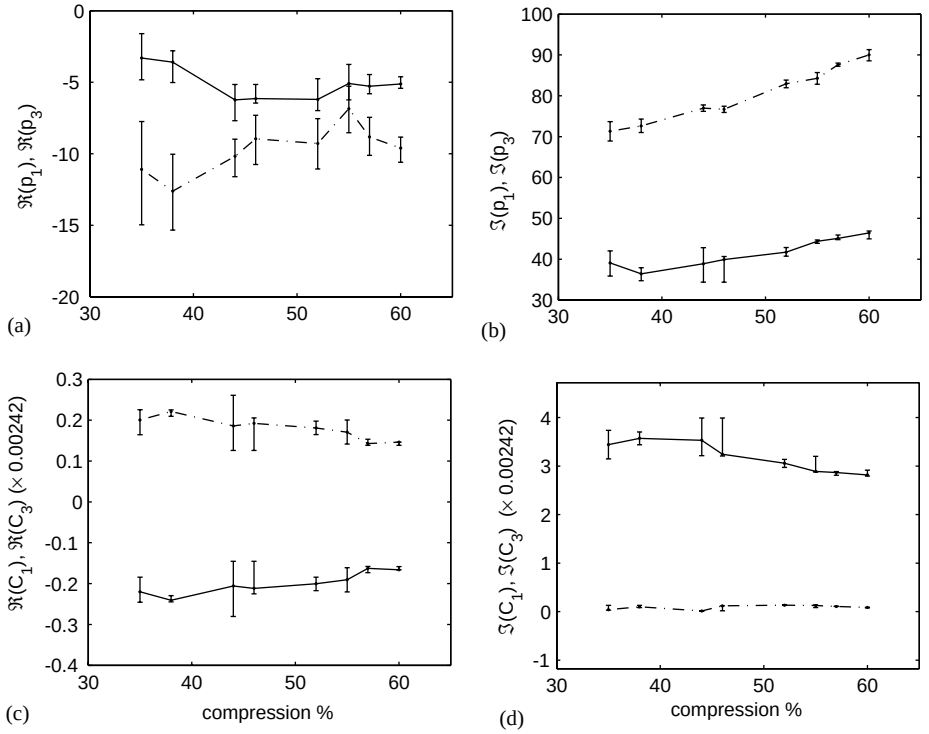

Fig. 16. The variation of the exponents p_j and the residues C_j with compression level. (a) $\Re(p_i)$, (b) $\Im(p_i)$, (c) $\Re(C_i)$, and (d) $\Im(C_i)$, where $i = 1, 3$. Solid lines denote the first component of response (p_1, C_1), and dashed lines denote the second component (p_3, C_3). $p_2 = \overline{p_1}$, $p_4 = \overline{p_3}$, $C_2 = \overline{C_1}$, and $C_4 = \overline{C_3}$.

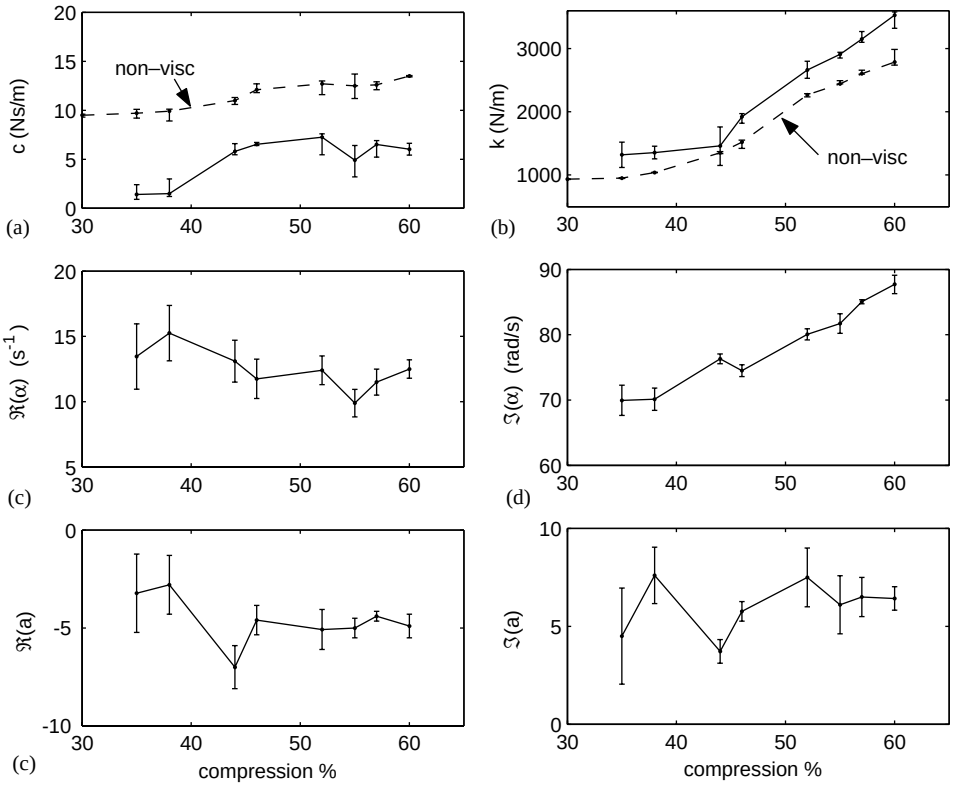

Fig. 17. The estimated values of the system parameters, along with their error bounds: (a) c (Ns/m), (b) k (N/m), (c)–(d) real and imaginary parts of α (s^{-1}), (e)–(f) real and imaginary parts of a (s^{-1}). c and k estimates are also given for the non-viscoelastic models, shown by dashed lines in (a) and (b) respectively.

parameters were also the most sensitive to experimental variations and thus exhibited larger variability than the other parameter estimates, obscuring any trends that may be present.

The $\Re(\alpha_i)$ can be interpreted as the inverse of the time constants associated with the foam, τ_i, that is, $\tau_i = 1/\Re(\alpha_i)$. Within the range of variability of estimates of $\Re(\alpha_i)$, their values, for all compression levels, appear to be almost constant and represent time constants in the range of 0.067–0.100 s.

6. Quasi-static creep experiment

To gain information about relatively longer time constants associated with the foam, a quasi-static creep test was performed. For this test, the foam block was loaded with a mass of 1.178 kg in the test fixture and its compression was measured over time using a Schaevitz-made linear variable differential transformer (LVDT) with a 2-in stroke length. The mass block was first brought in contact with the foam at zero velocity and then released, in order to provide zero initial conditions for the experiment. The measured quantity was displacement (creep) of the foam from its original state of zero compression. The response data was recorded at a sampling frequency of

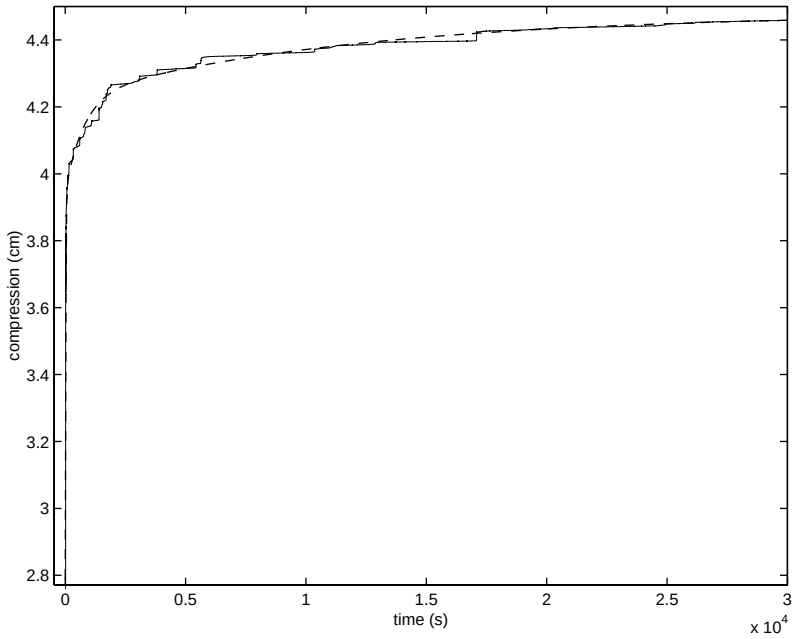

Fig. 18. The measured creep response (solid line) and a third order Prony series model response (dashed line).

0.5 Hz, for a duration of over 8 h. The creep response is shown in Fig. 18, along with a three-term Prony series used to fit the data. The measured response includes some discrete jumps in displacements, believed to be due to slip–stick behavior caused by dry friction in the fixture.

To obtain the three exponents, the data was downsampled to 0.03125 Hz, and model orders of 100–250 were used in the forward prediction stage (step 1) of the Prony series estimation. The positions of the three poles were estimated to be 0.9972 and 0.9593 and 0.2327 on the real axis in complex plane, and were picked because of their good clustering behavior. The poles correspond to time constants of 3.29 h, 12.84 min, and 22 s, respectively. Owing to the poor quality of experimental data, the estimates of the time constants are not accurate. Specifically, the latter two could be as large as 48 min and 55 s, respectively, depending upon which model orders were used. While somewhat imperfect due to the presence of dry friction, this test demonstrates the existence of very long time constants in the response of polyurethane foam. These time constants are not identified when using the impulse tests. This supports the observed behavior that the foam block, when loaded with a mass block, takes a long time to reach its static equilibrium. Typically, a duration of about 8 h was required for the considered system to reach its steady state of 52% compression.

7. Summary and conclusions

A method for the identification of the parameters of a linear, dynamical, single degree of freedom, viscoelastic system was presented. The viscoelastic term in the model is a convolution of

the response with a sum-of-exponentials kernel function. The identification method utilizes the free response of a system responding to an impact and is based on Prony series modelling of this response. Pole locations and model order are determined by fitting high order models to a time-reversed response history and identifying clusters in pole maps. Further verification of pole location came from using responses from multiple tests. The Prony series parameter estimates were then used to determine the material parameters, a two-step processes requiring identification of the exponents in the viscoelastic kernel followed by a least-squares solution to a set of linear equation. Effects of dry friction and noise and the difficulties of estimating the parameters of closely spaced, weak, and fast or slow decaying modes were discussed. The technique was applied to identifying the material parameters of polyurethane foam pre-compressed to various levels. The long memory of the foam, its sensitivity to ambient temperature and humidity, and its non-linear stiffness characteristics all influence the response, and thus an experimental procedure to produce repeatable results in the foam testing was established. Prony series models were also used to model long-term static creep behavior, though dry friction effects in the foam testing fixture affected the accuracy of these results.

The method could be successfully applied to the identification of foam. A two-term kernel function resulted in a reasonable model of the system, but there is evidence that perhaps an even higher number of terms are required in the kernel to fully model the response time history. However, inclusion of these terms resulted in poles that are so close that the Prony series method does not identify them as separate pole clusters. Their presence was revealed only when examining pole drift at very high model orders. This effect was confirmed through realistic simulations of the response. However, by increasing the model order, it will always be possible to improve the model fit to the data, thus the validity of mass-foam system models with closely spaced components should be investigated further.

The impulse testing with a two-term kernel model resulted in time constants between 0.067 and 0.1 s, and pole clustering from modelling the response of the creep test resulted in the identification of three strong components with time constants around 20 s, 13 min, and 3.5 h. Clearly, there is a gap between these groups of time constants, and methods to identify whether time constants between 0.1 and 20 s exist should be developed. Modelling the creep response closer to the application of the mass does reveal shorter time constants but the lack of data at this location make their estimation problematic. The relationship between the time constants of the viscoelastic kernel terms and the time constants associated with the modes present in the response is complicated, as illustrated in Fig. 7. If parameter combinations result in weak, fast decaying or slow decaying free response modes, these may be difficult to identify accurately, if at all. Poor identification at this stage will result in extremely poor estimation of the material properties.

Applying the model with the two-term viscoelastic kernel to foam at different compressions revealed a growth in viscous damping (c), stiffness (k), and the frequency of the exponential in the viscoelastic kernel, as the compression increased from 35% to 60%. Any variation in the other parameters was not present or obscured by the variance of the parameter estimates. In future, the method will be applied to a variety of foams to detect how the parameters vary as a function of material and processing parameters, and to further assess the accuracy and robustness of the identification process. The steady state response of this system to harmonic excitation when non-linearities in the foam's elastic properties are excited is also being studied through the use of harmonic balance models.

Acknowledgements

The authors acknowledge the support of Dr. Alison Flatau through NSF Grant 9900248-CMS, and the technical and financial support of Dr. Bryan McKinney and Mr. Kuntal Thakurta, at ASG, Johnson Controls Inc. We also acknowledge the support and encouragement given by Dr. D.K. Showers and Mr. P.E. Liedtke in our work.

Appendix A. Derivation of roots of Eq. (13) for $N = 1$

It was discussed in Section 3.1 that Eq. (17) yields $N + 1$ roots for N unknowns. The spurious root was reported to be related to the initial conditions x_0 and $\dot{x}_0$. For the case of $N = 1$, the proof is presented below.

For $N = 1$, Eq. (17) becomes

$$A_0\beta^2 + A_1\beta + A_2 = 0, \tag{A.1}$$

where, using Eq. (14), the coefficients A_0, A_1, and A_2 become

$$A_0 = C_1 + C_2 + C_3, \tag{A.2a}$$

$$A_1 = C_1(p_2 + P_3) + C_2(p_1 + p_3) + C_3(p_1 + p_2), \tag{A.2b}$$

$$A_2 = C_1p_2p_3 + C_2p_3p_1 + C_3p_1p_2. \tag{A.2c}$$

C_j, and $p_j, j = 1, 2, 3$, are the response coefficients for $N = 1$. The coefficients A_0, A_1, and A_2 need to be expressed as functions of system parameters and the initial conditions. For this purpose, note that the initial conditions are related to C_j and p_j as

$$C_1 + C_2 + C_3 = x_0, \tag{A.3a}$$

$$C_1p_1 + C_2p_2 + C_3p_3 = \dot{x}_0. \tag{A.3b}$$

The exponents p_j are the roots of the characteristic equation of the system for $N = 1$. Hence

$$mp_j^2 + cp_j + k - k\frac{a}{p_j + \alpha} = 0, \quad j = 1, 2, 3, \tag{A.4}$$

which can be re-written as

$$mp_j^3 + (c + m\alpha)p_j^2 + (k + c\alpha)p_j + k(\alpha - a) = 0 \quad (\text{for } p_j \neq \alpha). \tag{A.5}$$

The exponents p_j can be related to the coefficients of Eq. (A.5) as

$$p_1 + p_2 + p_3 = -\alpha - \frac{c}{m}, \tag{A.6a}$$

$$p_1p_2 + p_3p_1 + p_2p_3 = \frac{k + c\alpha}{m}, \tag{A.6b}$$

$$p_1p_2p_3 = -\frac{k}{m}(\alpha - a). \tag{A.6c}$$

Thus we have

$$A_0 = x_0, \tag{A.7}$$

$$\begin{aligned} A_1 &= (C_1 + C_2)p_3 + (C_2 + C_3)p_1 + (C_3 + C_1)p_2 \\ &= (x_0 - C_3)p_3 + (x_0 - C_1)p_1 + (x_0 - C_2)p_2 \\ &= x_0(p_1 + p_2 + p_3) - (C_1p_1 + C_2p_2 + C_3p_3) \\ &= -x_0\left(\alpha + \frac{c}{m}\right) - \dot{x}_0, \end{aligned} \tag{A.8}$$

$$\begin{aligned} A_2 &= (x_0 - C_2 - C_3)p_2p_3 + (x_0 - C_3 - C_1)p_3p_1 + (x_0 - C_1 - C_2)p_1p_2 \\ &= x_0(p_1p_2 + p_3p_1 + p_2p_3) \\ &\quad - \{(C_1p_1 + C_2p_2)p_3 + (C_2p_2 + C_3p_3)p_1 + (C_3p_3 + C_1p_1)p_2\} \\ &= x_0\left(\frac{k + c\alpha}{m}\right) \\ &\quad - \{\dot{x}_0(p_1 + p_2 + p_3) - (C_1p_1^2 + C_2p_2^2 + C_3p_3^2)\} \\ &= x_0\left(\frac{k + c\alpha}{m}\right) + \dot{x}_0\left(\alpha + \frac{c}{m}\right) \\ &\quad + (C_1p_1^2 + C_2p_2^2 + C_3p_3^2). \end{aligned} \tag{A.9}$$

Multiplying Eq. (A.4) by C_j and summing up for all j yields:

$$\sum_{j=1}^{3} C_jp_j^2 = -\frac{c}{m}\sum_{j=1}^{3} C_jp_j - \frac{k}{m}\sum_{j=1}^{3} C_j + \frac{ka}{m}\sum_{j=1}^{3}\frac{Cj}{\alpha + p_j}. \tag{A.10}$$

Using Eqs. (13) and (A.3) in Eq. (A.10), we get

$$\sum_{j=1}^{3} C_jp_j^2 = -\frac{c}{m}\dot{x}_0 - \frac{k}{m}x_0. \tag{A.11}$$

Using this expression for $\sum_j C_jp_j^2$ in Eq. (A.9) gives:

$$A_2 = \alpha\dot{x}_0 + \frac{\alpha c}{m}x_0. \tag{A.12}$$

By using expressions for A_0, A_1, and A_2 in Eq. (A.1) and simplifying

$$x_0(\beta - \alpha)\left(\beta - \frac{c}{m} - \frac{\dot{x}_0}{x_0}\right) = 0. \tag{A.13}$$

If $x_0 \neq 0$, this equation yields two roots

$$\hat{\beta}_1 = \alpha, \tag{A.14}$$

$$\hat{\beta}_2 = \frac{c}{m} + \frac{\dot{x}_0}{x_0}. \tag{A.15}$$

$\hat{\beta}_2$ is the spurious root. When $x_0 = 0$, this root does not arise because $A_0 \equiv 0\ \forall N$, and hence Eq. (17) is of order N. The expression for the spurious root remains the same for other values of N

also. This can be shown by substituting Eq. (A.15) into the left-hand side of Eq. (17) and proving that the result is zero.

References

[1] K.D. Cavender, Real time foam performance testing, Journal of Cellular Plastics 29 (1993) 350–363.
[2] J.W. Leenslag, E. Huygens, A. Tan, Recent advances in the development and characterization of automotive comfort seating foams, Polyurethanes World Congress 1997, Amsterdam, September 29–October 1, 1997, pp. 436–446.
[3] N.C. Hilyard, W.L. Lee, A. Cunningham, Energy dissipation in polyurethane cushion foams and its role in dynamic comfort, Cellular Polymers, Forum Hotel, London, RAPRA Technology Ltd., 1991, pp. 187–191.
[4] J.C. Moreland, G.L. Wilkes, R.B. Turner, Viscoelastic behavior of flexible slabstock polyurethane foams: dependence on temperature and relative humidity. I. Tensile and compression stress (load) relaxation, Journal of Applied Polymer Science 52 (1994) 549–568.
[5] J.C. Moreland, G.L. Wilkes, R.B. Turner, Viscoelastic behavior of flexible slabstock polyurethane foams: dependence on temperature and relative humidity. II. Compressive creep behavior, Journal of Applied Polymer Science 52 (1994) 569–576.
[6] J.D. Ferry, Viscoelastic Properties of Polymers, Wiley, New York, 1970.
[7] F. Gandhi, I. Chopra, A time-domain non-linear viscoelastic damper model, Smart Materials and Structures 5 (1996) 517–528.
[8] B.B. Lodhia, I.I. Esat, Vibration simulation of systems incorporating linear viscoelastic mounts using Prony series formulation, American Society of Mechanical Engineers, Petroleum Division (Publication) 81 (1996) 171–176.
[9] B.D. Coleman, W. Noll, Foundations of linear viscoelasticity, Review of Modern Physics 33 (2) (1961) 239–249.
[10] M.K. Neilsen, R.D. Krieg, H.L. Schreyer, A constitutive theory for rigid polyurethane foam, Polymer Engineering and Science 35 (5) (1995) 387–394.
[11] W. Flugge, Viscoelasticity, Blaisdell, Waltham, MA, 1967.
[12] N.W. Tschoegl, The Phenomenological Theory of Linear Viscoelastic Behavior, Springer, Berlin, 1989.
[13] C. Carrot, V. Verney, Determination of a discrete relaxation spectrum from dynamic experimental data using the Padé-Laplace method, European Polymer Journal 32 (1) (1996) 69–77.
[14] S.W. White, S.K. Kim, A.K. Bajaj, P. Davies, D.K. Showers, P.E. Liedtke, Experimental techniques and identification of nonlinear and viscoelastic properties of flexible polyurethane foam, Nonlinear Dynamics 22 (2000) 281–313.
[15] A. Muravyov, S.G. Hutton, Closed-form solutions and the eigenvalue problem for vibration of discrete viscoelastic systems, Journal of Applied Mechanics 64 (1997) 684–691.
[16] S.L. Marple, Digital Spectral Analysis With Applications, Prentice-Hall, Englewood Cliffs, NJ, 1987.
[17] P. Yu, Y.M. Haddad, A dynamic system identification method for the characterization of the rheological response of a class of viscoelastic materials, International Journal of Pressure Vessels and Piping 61 (1994) 87–97.
[18] P. Yu, Y.M. Haddad, On the dynamic system identification of the response behaviour of linear viscoelastic materials, International Journal of Pressure Vessels and Piping 67 (1996) 45–54.
[19] C.S. Ramalingam, R. Kumaresan, D. van Ormondt, New pole-by-pole model fitting approach for signal parameter estimation, Proceedings of the IEEE International Conference on Acoustics, Speech and Signal Processing 5 (1991) 3409–3412.
[20] M.H. Hayes, Statistical Digital Signal Processing and Modeling, Wiley, New York, 1996.
[21] R. Kumaresan, D.W. Tufts, Estimating the parameters of exponentially damped sinusoids and pole-zero modeling in noise, IEEE Transactions on Acoustics, Speech and Signal Processing 30 (6) (1982) 833–840.
[22] R. Kumaresan, D.W. Tufts, L.L. Scharf, A Prony method for noisy data: choosing the signal components and selecting the order in exponential signal models, Proceedings of the IEEE 72 (2) (1984) 230–233.
[23] S.G. Braun, Y.M. Ram, Structural parameter-identification in the frequency-domain—the use of overdetermined systems, Journal of Dynamic Systems Measurement and Control-Transactions of the American Society of Mechanical Engineers 109 (2) (1987) 120–123.

[24] A.V. Oppenheim, R.W. Schafer, Discrete-Time Signal Processing, Prentice-Hall, Englewood Cliffs, NJ, 1989.
[25] A. Ducasse, C. Mailhes, F. Castanie, Amplitude and phase estimator study in Prony method for noisy exponential data, Proceedings of the IEEE International Conference on Acoustics, Speech and Signal Processing, 3: Statistical Signal and Array Processing (1995) 1796–1799.
[26] A. Muravyov, S.G. Hutton, Free vibration response characteristics of a simple elasto-hereditary system, Journal of Vibration and Acoustics-Transactions of the American Society of Mechanical Engineers 120 (1998) 628–632.
[27] S.Y. Kung, K.S. Arun, D.V. Bhaskar Rao, State-space and singular-value decomposition-based approximation methods for the harmonic retrieval problem, Journal of the Optical Society of America 73 (12) (1983) 1799–1811.
[28] S.V. Huffel, H. Chen, C. Decanniere, P.V. Hecke, Algorithm for time-domain NMR data fitting based on total least squares, Journal of Magnetic Resonance Series A 110 (2) (1994) 228–237.
[29] R.G. Martin, M.C.C. Perez, Extended Prony method applied to noisy data, Electronic Letters 22 (11) (1986) 613–614.
[30] L. Dietrich, T. Lekszycki, K. Turski, Problems of identification of mechanical characteristics of viscoelastic composites, Acta Mechanica 126 (1998) 153–167.
[31] F.S. Gant, M.V. Bower, Domain of influence method: a new method for approximating Prony series coefficients and exponents for viscoelastic materials, Journal of Polymer Engineering 17 (1) (1997) 1–21.
[32] S.W. Park, R.A. Schapery, Methods of interconversion between linear viscoelastic material functions. Part I—a numerical method based on Prony series, International Journal of Solids and Structures 36 (11) (1999) 1653–1675.
[33] S.V. Krysov, V.A. Lazarev, To the Adirovich and Blokhintsev dry friction model. Consideration of material viscoelastic properties, Soviet Journal of Friction and Wear 13 (2) (1992) 251–256.
[34] R. Singh, P. Davies, A.K. Bajaj, Initial condition response of a viscoelastic dynamical system in the presence of dry friction and identification of system parameters, Journal of Sound and Vibration 239 (5) (2001) 1086–1095.
[35] J.W. Liang, B.F. Feeny, Identifying coulomb and viscous friction from free-vibration decrements, Nonlinear Dynamics 16 (1998) 337–347.